Tensor-based numerical method for stochastic homogenisation

Quentin Ayoul-Guilmard[*1], Anthony Nouy[†2], and Christophe Binetruy[1]

[1]École Centrale de Nantes, GeM UMR CNRS 6183, Nantes, France
[2]École Centrale de Nantes, LMJL UMR CNRS 6629, Nantes, France

Abstract

This paper addresses the complexity reduction of stochastic homogenisation of a class of random materials for a stationary diffusion equation. A cost-efficient approximation of the correctors is built using a method designed to exploit quasi-periodicity. Accuracy and cost reduction are investigated for local perturbations or small transformations of periodic materials as well as for materials with no periodicity but a mesoscopic structure, for which the limitations of the method are shown. Finally, for materials outside the scope of this method, we propose to use the approximation of homogenised quantities as control variates for variance reduction of a more accurate and costly Monte Carlo estimator (using a multi-fidelity Monte Carlo method). The resulting cost reduction is illustrated in a numerical experiment with a control variate from weakly stochastic homogenisation for comparison, and the limits of this variance reduction technique are tested on materials without periodicity or mesoscopic structure.

1 Introduction

Many industries show a growing interest in heterogeneous materials designed with a regular—even periodic—microscopic structure, such as most composite materials. Prediction of the behaviour of such materials, either during production or intended use, raises various challenges. Amongst those is the computational complexity induced by the scale difference between the size of the final component and the micro-structure that has to be represented. Multiscale complexity is a long-standing topic for which various well documented methods such as Multiscale Finite Elements Method [MsFEM, explained in 15], Heterogeneous Multiscale Method [HMM, see 1] have been developed. Unlike those general methods, a method designed specifically to break this complexity by exploiting quasi-periodicity was recently proposed by Ayoul-Guilmard et al. [5].

Another long-standing approach to tackle this issue is to substitute a homogenised material in the simulations; even though some detailed information is lost, this is still a relevant strategy

---

[*]quentin.ayoul-guilmard@centraliens-nantes.net
[†]anthony.nouy@ec-nantes.fr

for many quantities of interest, as discussed by Murat et al. [in 26]. Although low for periodic materials, the homogenisation cost rises significantly with random periodicity loss [see e.g. 21]. This is a barrier to random defect modelling in these simulations.

We propose in this paper to tackle this issue with an approximation of the corrector functions, the computation of which is the costliest part of the homogenisation process, using the method from Ayoul-Guilmard et al. [5]. Section 2 will introduce the necessary background on homogenisation for heterogeneous diffusion. Section 3 will present the key points of the approximation method and illustrate its performance and limits on various numerical experiments.In order to improve on the accuracy of this surrogate model, we propose in section 4 to combine it with another, costlier and more precise, within a multi-fidelity Monte Carlo method [such as described in 31]. Its performance is compared with another surrogate model from Legoll and Minvielle [22].

2   Periodic and stochastic homogenisation

2.1   General homogenisation

Let $D \subset \mathbb{R}^d$ an open bounded domain. We consider an heterogeneous stationary diffusion problem

$$-\nabla \cdot (K \nabla u) = f, \tag{2.1}$$

$$u_{|\partial D} = 0, \tag{2.2}$$

with $f \in H^{-1}(D)$. K is assumed to have variations at a small scale on D, which makes practical computations expensive. We wish to substitute to (2.1) a problem without such variations that preserves certain quantities of interest. For any $0 < \alpha < \beta$ we let,

$$\mathcal{M}(\alpha, \beta) := \left\{ a \in L^\infty(D; \mathbb{R}^{d \times d}) : \langle a(x)y \,|\, y \rangle \geqslant \alpha \|y\|^2 \right.$$
$$\left. \text{and } \|a(x)y\| \leqslant \beta \|y\|, \forall y \in \mathbb{R}^d, \text{ for a.e. } x \in D \right\}.$$

Definition 1 (H-convergence). Let $f \in H^{-1}(D)$, $(K_n)_{n \in \mathbb{N}} \in \mathcal{M}(\alpha, \beta)^{\mathbb{N}}$ and $K_\star \in \mathcal{M}(\alpha', \beta')$ with $0 < \alpha < \beta$ and $0 < \alpha' < \beta'$. Let $u_\star \in H^1(D)$ be solution to

$$\begin{cases} -\nabla \cdot (K_\star \nabla u_\star) = f \\ (2.2) \end{cases} \tag{2.3}$$

and, for any $n \in \mathbb{N}$, let $u_n \in H^1(D)$ be solution to

$$\begin{cases} -\nabla \cdot (K_n \nabla u_n) = f \\ (2.2) \end{cases}$$

We say that $(K_n)_{n \in \mathbb{N}}$ H-converges to $K_\star$ and note $K_n \Rightarrow K_\star$ when

$$u_n \xrightarrow{H^1(D)} u_\star,$$

$$K_n \nabla u_n \xrightarrow{L^2(D; \mathbb{R}^d)} K_\star \nabla u_\star.$$

H-convergence is a generalisation by Murat et al. [26] of the G-convergence to non-symmetric operators. G-convergence was originally introduced by Spagnolo [32]. The reader may consult Defranceschi [13] for a detailed explanation of both.

Theorem 1 (Fundamental theorem of homogenisation). *Let $(K_n)_{n \in \mathbb{N}} \in \mathcal{M}(\alpha, \beta)^{\mathbb{N}}$ with $0 < \alpha < \beta$. There exists a subsequence $(K_{s(n)})_{n \in \mathbb{N}}$ and an operator $K_\star \in \mathcal{M}(\alpha, \beta^2 \alpha^{-1})$ such that*

$$
\begin{aligned}
K_{s(n)} &\Rightarrow K_\star, \\
K_{s(n)} \nabla u_{s(n)} \cdot \nabla u_{s(n)} &\rightharpoonup K_\star \nabla u_\star \cdot \nabla u_\star \ \text{weakly-}* \text{ in } \mathcal{D}'(\mathbb{R}^d), \\
\text{and} \ \int_D K_{s(n)} \nabla u_{s(n)} \cdot \nabla u_{s(n)} &\to \int_D K_\star \nabla u_\star \cdot \nabla u_\star,
\end{aligned}
$$

where $\mathcal{D}'(\mathbb{R}^d)$ denotes the space of distributions on $\mathbb{R}^d$. $K_\star$ is commonly called the "homogenised operator" of K.

Proof. See Murat et al. [26, pp. 31–36]. $\qquad\qquad\square$

Theorem 2 (Corrector theorem). *Let $(K_n)_{n \in \mathbb{N}} \in \mathcal{M}(\alpha, \beta)^{\mathbb{N}}$ with $0 < \alpha < \beta$. For any $i \in \{1, \ldots, d\}$, there exists a sequence $(w_n^i)_{n \in \mathbb{N}} \in H^1(D)^{\mathbb{N}}$ such that*

$$
w_{s(n)}^i \xrightarrow{H^1(D)} 0,
$$

$$
-\nabla \cdot \left(K_{s(n)}(e_i + \nabla w_{s(n)}^i) \right) \xrightarrow{H^{-1}(D)} 0,
$$

$$
\text{and} \ \nabla u_{s(n)} - (\mathrm{Id} + \nabla w_{s(n)}) \nabla u_\star \xrightarrow{L^1(D)^d} 0 \tag{2.4}
$$

where s defines the same subsequence as in [theorem 1](#). These functions w_n^i are called "correctors" for they provide the necessary correction to $\nabla u_{s(n)}$, in the sense of [(2.4)](#), to converge strongly towards $\nabla u_\star$. Additionally, they can be used to deduce $\nabla u_{s(n)}$ from $\nabla u_\star$. A direct consequence is that

$$
K_{s(n)}(\mathrm{Id} + \nabla w_{s(n)}) \xrightarrow{L^2(D)^{d \times d}} K_\star.
$$

Proof. See Murat et al. [26, pp. 37–42]. $\qquad\qquad\square$

2.2 Periodic homogenisation

The corrector functions introduced above are used to build the homogenised operator, but more information on K is required to give an expression of $K_\star$. The quasi-periodicity we are interested in arises most often as the result of random perturbation of a periodic medium, and both the periodic and stochastic context are well documented. Let us first consider the case where K is a periodic operator.

Proposition 1 (Periodic homogenisation). *Let $K \in \mathcal{M}(\alpha, \beta)$, with $0 < \alpha < \beta$, be periodic of period $Y \subset \mathbb{R}^d$. Let $(\epsilon_n)_{n \in \mathbb{N}} \in]0, +\infty[^{\mathbb{N}}$ be a sequence converging to 0. Then the results from [theorems 1](#) and [2](#) hold for the sequence $(K(\frac{\cdot}{\epsilon_n}))_{n \in \mathbb{N}}$ itself—not only on a subsequence. Furthermore,*

$$
\forall (i, j) \in \{1, \ldots, d\}^2, \ (K_\star)_{ij} = \int_Y (e_i + \nabla w_i) \cdot K e_j, \tag{2.5}
$$

where the corrector $w_i \in H^1_\sharp(Y) := \{ v \in H^1(Y) : v \text{ is } Y\text{-periodic} \}$ solves

$$
-\nabla \cdot (K(e_i + \nabla w_i)) = 0. \tag{2.6}
$$

Proof. This result has been proven by different methods: first in 1978 through compensated compactness by Murat [25], then in 1979 with oscillating test functions by Tartar [33] and later in 1989 via two-scale convergence by Nguetseng [27]. □

The additional periodicity hypothesis in proposition 1 gives us expression (2.5) to compute the homogenised operator $K_\star$. The d corrector problems (2.6) to be solved are limited to the period Y, hence the reasonable cost. Additionally, this homogenisation is independent of the source term f and the boundary conditions, since they do not affect the homogenised operator, and are identical in both the original problem (2.1)–(2.2) and the homogenised one (2.3). This justifies the concept of "homogenised material".

2.3   Stochastic homogenisation

In the case where K is stochastic, the general results from theorems 1 and 2 hold almost surely. We introduce a probability space $(\Omega, \mathcal{E}, \mathbb{P})$. Stochastic homogenisation generally relies on a stationarity assumption, i.e. invariance of probability laws with respect to space (or time) translation. We expect K to have a spatial quasi-periodic structure, therefore we choose a definition of stationarity suited to represent such structure.

Definition 2 (Discrete stationarity)**.** Let us assume that the group $(\mathbb{Z}^d, +)$ acts on $(\Omega, \mathcal{E}, \mathbb{P})$ through an ergodic measure-preserving transformation $\tau = (\tau_z)_{z \in \mathbb{Z}^d}$:

$$\forall e \in \mathcal{E}, \quad [\forall z \in \mathbb{Z}^d, \tau_z e = e] \to [\mathbb{P}(e) \in \{0, 1\}].$$

Any $\phi \in L^1_{loc}(\mathbb{R}^d; L^1(\Omega))$ is said to be (discretely) stationary if, and only if,

$$\forall z \in \mathbb{Z}^d, \phi(x + z, \omega) = \phi(x, \tau_z \omega) \text{ a.e. on } \mathbb{R}^d \times \Omega.$$

We can observe that the probability law of a function ϕ, stationary in the sense of definition 2, is invariant by any translation by $z \in \mathbb{Z}^d$: since τ_z is preserves the measure, $\phi(x, \cdot)$ and $\phi(x + z, \cdot)$ follow the same probability law. This is related to periodicity, e.g. any stationary function has a Y-periodic expectation, where $Y := [0, 1]^d$. Up to a linear mapping $x \mapsto x/\varepsilon$, we can relate any $[0, \varepsilon]^d$-periodic function to definition 2. It should be noted that discrete stationarity is not a particular case of continuous stationarity.

Henceforth, stationarity will be meant in the discrete sense defined above and K is assumed to be stationary. This definition, albeit not used directly here, allows us to use some well-known results of stochastic homogenisation, such as the ergodic theorem formulated below in this discrete setting.

Theorem 3 (Ergodic theorem)**.** *Let* $K \in L^\infty(\mathbb{R}^d; L^1(\Omega))$ *be stationary. Then we have almost surely*

$$\frac{1}{(2N+1)^d} \sum_{\|z\|_\infty \leqslant N} K(x, \tau_z \omega) \xrightarrow[N \to \infty]{L^\infty(\mathbb{R}^d)} \mathbb{E}(K(x, \cdot))$$

$$\text{and } K\left(\frac{x}{N}, \omega\right) \xrightarrow[N \to \infty]{L^\infty(\mathbb{R}^d)} \mathbb{E}\left(\int_Y K\right) \quad \text{in weak-* topology.}$$

Proof. See Birkhoff [7]. □

Proposition 2 (Stochastic homogenisation)**.** *Let* $K \in L^\infty(\mathbb{R}^d; L^1(\Omega))$ *be stationary and such that* $K(\cdot, \omega) \in \mathcal{M}(\alpha, \beta)$*, with* $0 < \alpha < \beta$*, almost surely. Let* $(\epsilon_n)_{n \in \mathbb{N}} \in]0, +\infty[^\mathbb{N}$ *be a sequence*

converging to 0. *Then the results from theorems 1 and 2 hold for a subsequence of* $(K(\frac{\cdot}{\epsilon_n}, \cdot))_{n \in \mathbb{N}}$. *Furthermore,*

$$\forall (i,j) \in \{1, \ldots, d\}^2, \ (K_\star)_{ij} = \mathbb{E}\left(\int_Y (e_i + \nabla w_i) \cdot K e_j\right),$$

where[1] every corrector $w_i \in \mathcal{W}$ *is solution to*

$$\begin{cases} -\nabla \cdot (K(e_i + \nabla w_i)) &= 0 \ \text{a.s. on } \mathbb{R}^d \\ \mathbb{E}\left(\int_Y \nabla w_i\right) &= 0 \\ \nabla w_i \ \text{stationary} \end{cases} \tag{2.7}$$

Proof. See Jikov et al. [21, th. 7.9, p. 244]. □

Unlike the periodic corrector problems (2.6), the stochastic corrector problems (2.7) are impractical to solve because of the global conditions over both $\mathbb{R}^d$ and Ω. This is why practical computations of $K_\star$ usually introduce the "apparent homogenised operator"

$$(K_\star^N)_{ij} := \int_{Y_N} (e_i + \nabla w_{N,i}) \cdot K \cdot e_j \tag{2.8}$$

on a truncated domain $Y_N = [0, N]^d$, where the "apparent correctors" are solutions to

$$\begin{cases} -\nabla \cdot (K(e_i + \nabla w_{N,i})) &= 0 \quad \text{a.s. on } Y_N \\ w_{N,i} \ Y_N\text{-periodic} \end{cases} \tag{2.9}$$

Since K is stationary, theorem 3 yields [see 10, th. 1 p. 158]

$$\mathbb{E}(K_\star^N) = \lim_{N \to \infty} K_\star^N = K_\star, \tag{2.10}$$

therefore we can approximate $K_\star$ with a Monte Carlo estimator

$$\theta_m(K_\star^N) := \frac{1}{m} \sum_{i=1}^m K_\star^N(\cdot, \omega_i) \tag{2.11}$$

of $\mathbb{E}(K_\star^N)$, using m samples (independent and identically distributed) $K(\cdot, \omega_i), 1 \leqslant i \leqslant m$. The chain of approximation thus reads $K_\star \approx \mathbb{E}(K_\star^N) \approx \theta_m(K_\star^N)$. An evaluation of this estimator requires $d \times m$ resolutions of the apparent corrector problem (2.9), which remains considerably more expensive than periodic homogenisation. Furthermore,

$$\left\| \mathbb{E}(K_\star^N) - \theta_m(K_\star^N) \right\|_{L^2(\Omega)} = \sqrt{\frac{\mathbb{V}\mathrm{ar}(K_\star^N)}{m}}, \tag{2.12}$$

so the rate of convergence of the estimator is rather slow; hence the benefit of a method to exploit quasi-periodicity in order to break down the complexity of these corrector problems.

---

[1]We let $\mathcal{W} := \left\{ v \in L^2_{loc}(\mathbb{R}^d; L^2(\Omega)) : \nabla v \in L^2_{unif}(\mathbb{R}^d; L^2(\Omega)) \right\}$ with $L^2_{unif}(\mathbb{R}^d; L^2(\Omega)) := \left\{ v \in L^2(\mathbb{R}^d; L^2(\Omega)) : \exists C \in \mathbb{R}_{+*}, \forall x \in \mathbb{R}^d \times \mathbb{R}_{+*}, \|v\|_{L^2(\mathcal{B}(x,1); L^2(\Omega))} \leqslant C \right\}$, and $\mathcal{B}(x, R)$ the ball of centre x and radius R.

2.4   Homogenisation with random mapping

Alternatively to the previous setting, one may consider the problem (2.1) to be set on a domain transformed by a random stationary diffeomorphism $\phi(\omega) : \mathbb{R}^d \to \mathbb{R}^d$ such that $K \circ \phi =: K_\sharp$ is Y-periodic. We can then write (2.1) as

$$-\nabla \cdot \left(K_\sharp \circ \phi^{-1}(\omega) \nabla u\right) = f. \tag{2.13}$$

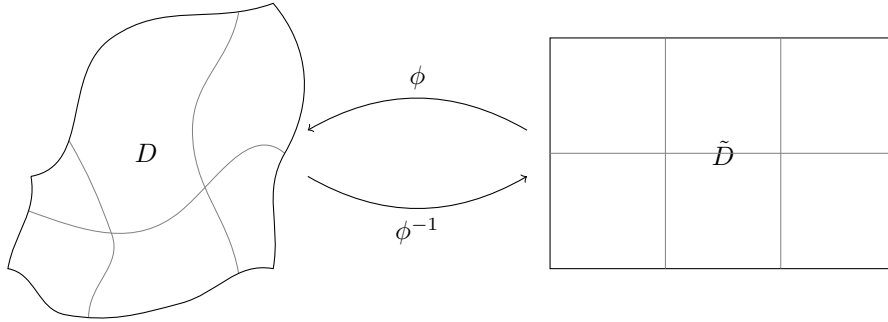This domain transformation is illustrated on figure 1.

Figure 1: Random mapping

Definition 3 (Random stationary diffeomorphism)**.** For $0 < \mu \leqslant \nu < +\infty$, let us note $\Phi(\mu, \nu)$ the set of functions $\varphi \in L^1(\Omega; C^1(\mathbb{R}^d, \mathbb{R}^d))$ such that, $\forall \omega \in \Omega$, $\varphi(\omega)$ is a.s. a diffeomorphism, $\nabla \varphi : \Omega \to C^0(\mathbb{R}^d; \mathbb{R}^{d \times d})$ (such that $\nabla \varphi(\omega)$ is the gradient of $\varphi(\omega)$) is stationary,

$$\underset{(x,\omega) \in \mathbb{R}^d \times \Omega}{\mathrm{Ess\,Inf}} \det(\nabla \varphi(\omega)(x)) \geqslant \mu, \qquad \text{and} \qquad \underset{(x,\omega) \in \mathbb{R}^d \times \Omega}{\mathrm{Ess\,Sup}} \|\nabla \varphi(\omega)(x)\| \leqslant \nu.$$

Proposition 3 (Homogenisation with random mapping)**.** *Let $K_\sharp \in \mathcal{M}(\alpha, \beta)$, with $0 < \alpha < \beta$, be periodic of period $Y \subset \mathbb{R}^d$; let $\phi \in \Phi(\mu, \nu)$, with $0 < \mu \leqslant \nu < +\infty$; let $(\epsilon_n)_{n \in \mathbb{N}} \in]0, +\infty[^{\mathbb{N}}$ be a sequence converging to 0. For any $n \in \mathbb{N}$, we note u_n the solution in $H^1(D)$ to*

$$\begin{cases} -\nabla \cdot \left(K_\sharp \circ \phi(\omega)^{-1}\left(\dfrac{\cdot}{\epsilon_n}\right) \nabla u_n \right) = f \\ u_{n|\partial D} = 0 \end{cases}.$$

Then $u_n \xrightarrow{H^1(D)} u_\star$ and $u_n \xrightarrow{L^2(D)} u_\star$, a.s., where $u_\star$ is solution of the homogenised problem

$$-\nabla \cdot (K_\star \nabla u_\star) = f.$$

The homogenised operator's coefficients are defined as

$$(K_\star)_{ij} = \det\left(\mathbb{E}\left(\fint_Y \nabla \phi(\cdot)\right)\right)^{-1} \mathbb{E}\left(\fint_{\phi(\cdot)(Y)} (e_i + \nabla w_i) \cdot (K_\sharp \circ \phi(\cdot)^{-1}) e_j\right)$$

for all $(i,j) \in \{1, \ldots, d\}^2$. Each corrector w_i is the solution of

$$\begin{cases} -\nabla \cdot \left(K_\sharp \circ \phi(\cdot)^{-1}(e_i + \nabla w_i)\right) = 0 \\ \mathbb{E}\left(\fint_{\phi(\cdot)(Y)} \nabla w_i\right) = 0 \\ \nabla \tilde{w}_i \text{ is stationary} \quad (\tilde{w}_i \circ \phi(\cdot)^{-1} := w_i) \end{cases} \tag{2.14}$$

in $H^1(Y; L^2(\Omega))$, unique up to the addition of a random constant.

Proof. See Blanc et al. [8, § 1.3, pp. 719–722]. □

Remark 1 (Extension of proposition 3). Different assumptions on the operator in (2.13) may be considered. Results similar to proposition 3 have been proven by Blanc et al. [9, pp. 11–13], with assumption of ergodicity and stationarity, either continuous or discrete in the sense of definition 2. Let us recall that the periodic setting considered here is a particular case of the discrete stationary setting, but *not* of the continuous one.

We can see that problem (2.14) presents the same issues as problem (2.7) where practical computations are concerned. The previous method based on apparent correctors computed on truncated domains [detailed in 10] has been adapted to this setting by Costaouec et al. [12]. We introduce the apparent homogenised operator

$$(K_\star^N(\omega))_{ij} := \det\left(\frac{1}{|Y_N|}\int_{Y_N} \nabla \phi(\omega)\right)^{-1}$$
$$\times \frac{1}{|Y_N|}\int_{Y_N} e_i K_\sharp \cdot (e_j + {}^t(\nabla \phi(\omega))^{-1} \nabla \tilde{w}_j^N(\omega)) \det(\nabla \phi(\omega)),$$

computed from apparent correctors $\tilde{w}_i^N \in H^1_\sharp(Y_N)$. These are the solutions, unique up to an additive random constant, to

$$\int_{Y_N} \nabla \tilde{v} \nabla \phi^{-1} \cdot K(e_i + {}^t\nabla \phi^{-1} \nabla \tilde{w}_i^N) \det(\nabla \phi) = 0, \forall \tilde{v} \in H^1_\sharp(Y_N),$$

which is equivalent to $\quad \int_{Y_N} \nabla \tilde{v} \cdot \tilde{K}({}^t\nabla \phi e_i + \nabla \tilde{w}_i^N) = 0, \forall \tilde{v} \in H^1_\sharp(Y_N),$ (2.15)

with $\tilde{K} := \det(\nabla \phi) \nabla \phi^{-1} K_\sharp {}^t\nabla \phi^{-1}$.

It has been proven by Legoll and Thomines [23] that $K_\star^N \xrightarrow[N \to \infty]{\text{a.s.}} K_\star$ so we can use a Monte Carlo method to estimate $\mathbb{E}(K_\star^N)$ and therefore to get an approximation of $K_\star$, as in the previous setting.

3   Tensor-based two-scale method

3.1   Description of the method

We will briefly outline a method to get a cost-efficient approximation to the solution of stationary heterogeneous diffusion problems such as (2.9). This method has been introduced by Ayoul-Guilmard et al. [5].

We consider a multiscale representation which separates microscopic and mesoscopic information, the mesoscopic scale being that of the periods. The domain D is partitioned into cells D_i, each being a period of the reference periodic medium. Letting $I \subset \mathbb{N}$ be the cell index set and $Y \subset \mathbb{R}^d$ a reference period, $I \times Y$ is identified with $\bigcup_{i \in I} D_i$ (see figure 2) through the isomorphism $\zeta : I \times Y \ni (i, y) \mapsto y + b_i \in D$, with b_i such that $Y + b_i = D_i$ for any cell $D_i, i \in I$.

Likewise, $\mathbb{R}^D$ is isomorphic to $\mathbb{R}^I \otimes \mathbb{R}^Y$ with isomorphism Υ such that, for any $v \in \mathbb{R}^D$, we identify v with

$$\Upsilon(v) = \sum_{n=1}^{\#I} e_n^I \otimes (v \circ \zeta(n, \cdot)) \quad \text{i.e., } \forall(i, y) \in I \times Y, \; v(\zeta(i, y)) = \sum_{n=1}^{\#I} e_n^I(i) v(\zeta(n, y)), \quad (3.1)$$
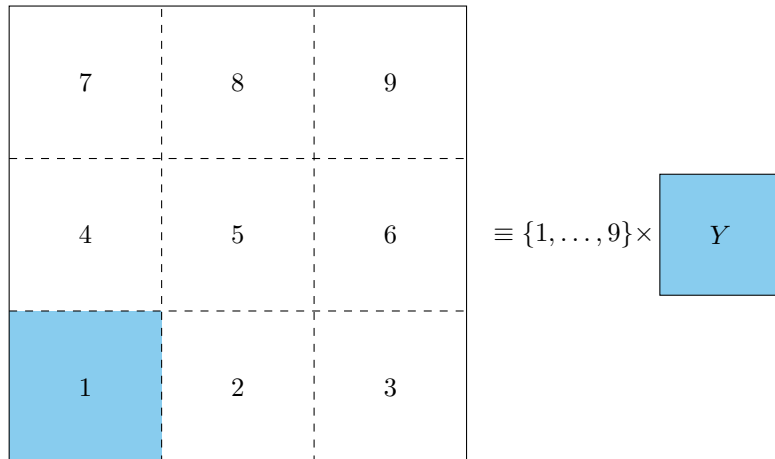
Figure 2: $D = \bigcup_{i \in I} D_i \equiv I \times Y$

where $\{e_n^I\}_{n \in I}$ is the canonical orthonormal basis of $\mathbb{R}^I$. Henceforth we will define the rank of v as the rank of $\Upsilon(v)$, which is the minimal r such that $\Upsilon(v) = \sum_{n=1}^r v_n^I \otimes v_n^Y$. More specifically, K and f can be identified with functions of $\mathbb{R}^I \otimes L^\infty(Y)$ and $\mathbb{R}^I \otimes L^2(Y)$, respectively, and the broken Sobolev space $H^1(\bigcup_{i \in I} D_i) = \{v \in L^2(\mathbb{R}) : \forall i \in I, v_{|D_i} \in H^1(D_i)\}$ is identified with $\mathbb{R}^I \otimes H^1(Y)$.

Consequently, problem (2.9) can be formulated over a space $V(D) \subset \mathbb{R}^I \otimes H^1(Y)$ within a discontinuous Galerkin setting[2]. This function space is defined as $V(D) := \mathbb{R}^I \otimes V(Y)$ with $V(Y) := \{v \in H^1(Y) : (\nabla v)_{|\partial Y} \in L^2(\partial Y)^d\}$. We then introduce a finite-dimensional subspace $V_h(D) := \mathbb{R}^I \otimes V_h(Y)$ with $V_h(Y) \subset V(Y)$ and look for an approximation of the corrector functions $w_{N,k}$ (with $N := \#I^{1/d}$) as solutions to

$$a_h^{swip}(w_{N,k}, \delta w) = b_{h,k}(\delta w), \ \forall \delta w \in V_h(D). \tag{3.2}$$

The benefit of format (3.1) lies in the match between the structure of the tensor product space and the underlying periodic organisation. The representation in $V(D)$ of a quasi-periodic function has as low a rank r as it is close to periodic. Note for example that a periodic function v is identified with a rank one tensor $\Upsilon(v) = 1^I \circ \varpi$, with $1^I : I \to \{1\}$ and $\varpi = v \circ \zeta(1, \cdot)$. The quasi-periodicity assumption on K is therefore interpreted as a low-rank assumption, hence our expectation that the solution of (3.2) would have a low rank. We exploit this by building a low-rank approximation of the solution of tensor-structured corrector problem (3.2) using a greedy algorithm [see 5, § 3.2]). The residual error is controlled with a tolerance ε so that

$$\frac{\left\| a_h^{swip}(w_{N,k}, \cdot) - b_{h,k} \right\|_{V_h(D)'}}{\|b_{h,k}\|_{V_h(D)'}} \leqslant \varepsilon. \tag{3.3}$$

Remark 2 (Random mapping). We assumed so far that the quasi-periodic structure of the medium (i.e. K) matches a perfectly regular mesoscopic mesh. The case where such mesh would be irregular, even random, can be addressed easily if we know a random stationary diffeomorphism ϕ such that $K \circ \phi =: K_\sharp$ is periodic; then, the results from subsection 2.4 apply. For this low-rank method to remain efficient, $\tilde{K}$ is assumed to have a low rank in $\mathbb{R}^I \otimes L^\infty(Y)$, which depends on

---

[2]with a SWIP method detailed in 14.

the ranks of $\nabla \phi^{-1}$ and $\det(\phi)$ (since $\operatorname{rank}(K_\sharp) = 1$). Remark 1 mentions that similar results can be proven for $K \circ \phi$ stationary, in which case the rank of $\tilde{K}$ is also influenced by the rank of $K \circ \phi$.

Modes recycling

An additional benefit arises from the tensor structure of $V(D)$ for successive simulations. One interpretation of format (3.1) is that

$$\forall i \in I, \quad v(i, \cdot) \in \operatorname{span}\left(v_n^Y\right)_{n \in \{1, \ldots, r\}},$$

so any function may be considered cell-wise as a superposition of the same set of microscopic patterns v_n^Y that we will call "modes". This concept is illustrated on figure 3: the nine modes in figure 3b compose the function pictured on figure 3a, where white lines delineate the hundred cells. Whenever the solutions to successive problems can be expected to evince similar modes, one may recycle those computed from one resolution to the next.

Such situation is common for random quasi-periodic materials, e.g. with sampling-based methods such as Monte Carlo estimation. Indeed, this strategy bears particular relevance if the differences between samples are consistent with the mesoscopic structure, which can be expected from our view of quasi-periodicity as a randomly perturbed periodicity. Since the perturbation is such that the rank of K remains low, recurring patterns are expected across realisations of K. Should those realisations differ mostly in their spatial distribution, then the conductivity's microscopic information remains unchanged and—expectedly—so does the solution's. Particularly, we will present in subsection 3.2 examples of problem (2.9) typical of such cases where only the functions $K_n^I \in \mathbb{R}^I$ in the representation $K \equiv \sum_n K_n^I \otimes K_n^Y$ are random[3]. Furthermore, this modes library is expected to reach a practical completion as a consequence of K's stationarity. I.e. the library will eventually become comprehensive enough to accurately represent the solution associated to almost any realisation of K, within the chosen tolerance.

The most straightforward implementation of this recycling strategy would be to set an anterior result $u_0 := \sum_{k=1}^{r_0} u_k^I \otimes u_k^Y$ as initial point for the subsequent resolution. Although the greedy algorithm would usually see its performance significantly improved by an initialisation close to the solution, it would always compute at least one additional term $u_{r_0+1}^I \otimes u_{r_0+1}^Y$, even if the two successive problems were identical. The resulting ever-growing library would yield worse performance than the original method. Therefore, we first look for a suitable approximation on the subspace spanned by the modes computed so far: we compute the Galerkin projection of u_0 on $\mathbb{R}^I \otimes \operatorname{span}\{u_1^Y, \ldots, u_{r_0}^Y\}$ then check the resulting approximation against criterion (3.3). If it is not satisfied, then said projection is set as the greedy algorithm's initial point. Once the library has reached its aforementioned practical completion, subsequent resolutions are reduced to this initial projection step, i.e. a Galerkin projection onto a subspace of $V_h(D)$ of which a basis is known and hopefully low-dimensional, thereby further reducing complexity.

This modes recycling strategy is akin to an adaptive reduced basis approach, and it should be noted that this basis construction strategy is non-optimal in the sense that the low-rank approximation is not optimal: the same precision might be achieved with a lower rank and yield a library of fewer modes. Although this non-optimal greedy algorithm is usually more cost-efficient as far as a single computation is concerned, this strategy has not been specifically designed toward library construction.

---

[3]In this specific case, operators over $V_h(Y)$ could be recycled as well, thus saving the associated assembling cost; since we observed this cost to be insignificant, we did not do so.
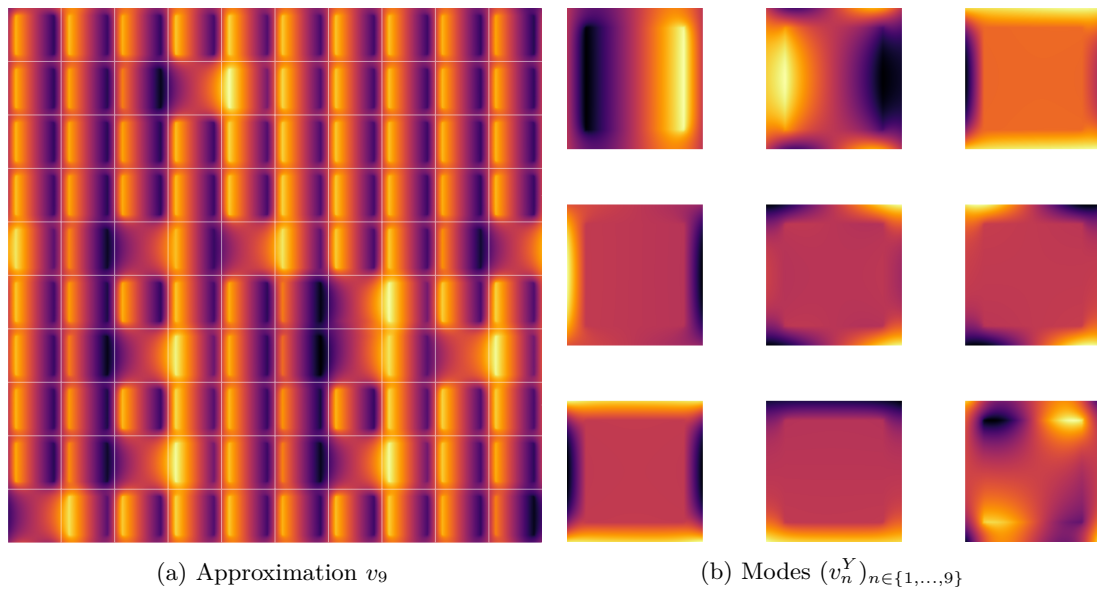
(a) Approximation v_9 (b) Modes $(v_n^Y)_{n \in \{1,\dots,9\}}$

Figure 3: Modes library example

3.2 Numerical examples

Each but the last of the following numerical experiments will involve an approximation of the homogenised conductivity $K_\star$ following the process described in subsection 2.3 with $D \subset \mathbb{R}^2$. The truncated corrector problems (2.9) will be solved using the multiscale low-rank method (MsLRM) outlined in subsection 3.1, and the homogenised conductivity will be approximated using a Monte Carlo estimator $\theta_m(K_\star^N)$ as expressed in equation (2.11). The number of samples $m = m(\eta)$ will be selected to satisfy the error criterion

$$\left\| \mathbb{E}(K_\star^N) - \theta_{m(\eta)}(K_\star^N) \right\|_{L^2(\Omega)} \leqslant \eta,$$

using equation (2.12) and an estimation of $\mathbb{V}\mathrm{ar}(\theta_{m(\eta)}(K_\star^N))$. We denote such an estimator $\theta^\eta := \theta_{m(\eta)}$. Unless specified otherwise, the default parameters values in table 1 apply to every experiment. These values will be discussed with experiments results below.

Table 1: Default tests parameters

N^2	$\dim(V_h(Y))$	ε	p	K_2/K_1	η
1600	441	0.01	0.1	100	0.05

The reference periodic medium of our main test case has a square inclusion in each cell, more conductive than the other phase, and the two phases have equal volume fractions. The random perturbation is the absence of some inclusions, replaced with the other phase. The random conductivity can be expressed as

$$K(i,y,\omega) = K_1 + B_i(\omega)\chi(y)(K_2 - K_1), \quad \forall (i,y,\omega) \in I \times Y \times \Omega, \tag{3.4}$$

where the random variables $(B_i)_{i \in I}$ follow independent and identical Bernoulli laws with $\mathbb{P}(B_i = 1) = p$, and $\chi : Y \to \{0,1\}$ is the characteristic function of the inclusion within the reference

cell. K is stationary according to definition 2. Figure 4 displays examples of such conductivity, associated correctors and source term, with the chosen reference cell $Y := [0,1]^2$ outlined on figure 4a. Every mesoscopic grid will be square unless specified otherwise.

Our reference when needed, both for accuracy and cost-efficiency evaluation, will be the exact same homogenisation process performed using a finite element method (FEM) with piecewise linear approximation for the corrector problems (2.9). For comparison purposes, its approximation space is built on an identical mesh, with the same degree of polynomials. This results in a problem of comparable size, if slightly smaller: a square domain of 400 cells with 400 finite elements each yield a FEM approximation space of dimension 160 801 and a tensor approximation space $V_h(D)$ of dimension 176 400.

All computations were run on the same workstation, i.e. a Dell$^{\mathrm{TM}}$ Optiplex$^{\mathrm{TM}}$ 7010 with:

- 8 GiB[4] (2×4) RAM DDR3 1600 MHz;

- Intel® Core$^{\mathrm{TM}}$ i7-3770 CPU: 4 cores at 3.40 GHz with 2 threads each.

3.2.1 Approximation precision

The trade-off between precision and cost-efficiency is fundamental to any approximation technique. We wish to assess the effect of MsLRM error on our quantity of interest $K_\star^N$. We computed the exact same[5] Monte Carlo estimator $\theta_{20}(K_\star^{20})$ by FEM and MsLRM, with different tolerances ε for MsLRM: 10^{-1}, 10^{-2}, 10^{-3}, 10^{-4} and 10^{-5}. FEM computational cost caused us to reduce the domain size and set an arbitrary low sample size, none of which interferes with the purpose of this test.

We can see on figure 5b how it affects the estimator's convergence, and it seems that a high tolerance shifts uniformly the estimation toward lower values: with inaccurately approximated correctors, the estimator underestimates the exact value (with a discrepancy apparently independent of m). Consequently, the error due to the approximation can not be compensated by a greater number of samples. We believe the cause to be an underestimation of the correctors' peaks at phase boundaries (visible on figures 4c and 4d as darker or lighter areas) so that the approximated correctors represent a medium with smaller conductivity jumps at phase boundary, hence a lower homogenised conductivity. However, we observe no significant accuracy improvement on the homogenised quantity beyond a tolerance of 10^{-3}: both the approximation of 10^{-3} and 10^{-5} seem as precise as the FEM reference. Even the approximation at 10^{-2} yields very close results.

Figure 5a shows the significant effect of ε on cost-efficiency: it is clear that reducing the tolerance increases considerably the computational cost. There seems to be a tipping point between 10^{-2} and 10^{-3} after which the cost increase is steeper. The tolerance value will be set to 10^{-2} henceforth as a satisfactory compromise.

3.2.2 Modes recycling

To illustrate modes recycling benefits, we computed the estimator $\theta^\eta(K_\star^N)$ with and without recycling. For the sake of graph clarity, only the first 20 samples were displayed on figure 6. We see on figure 6b the average corrector's rank per sample (averaged over both correctors). With recycling the average rank reaches immediately a plateau, which means the modes library was complete enough after the first sample. The computational cost is not reduced to zero however, as is shown on figure 6a. The larger the modes library, the higher the cost of initial step (i.e.

---

[4]5.5 to 6.5 of which were usually available for the simulations.
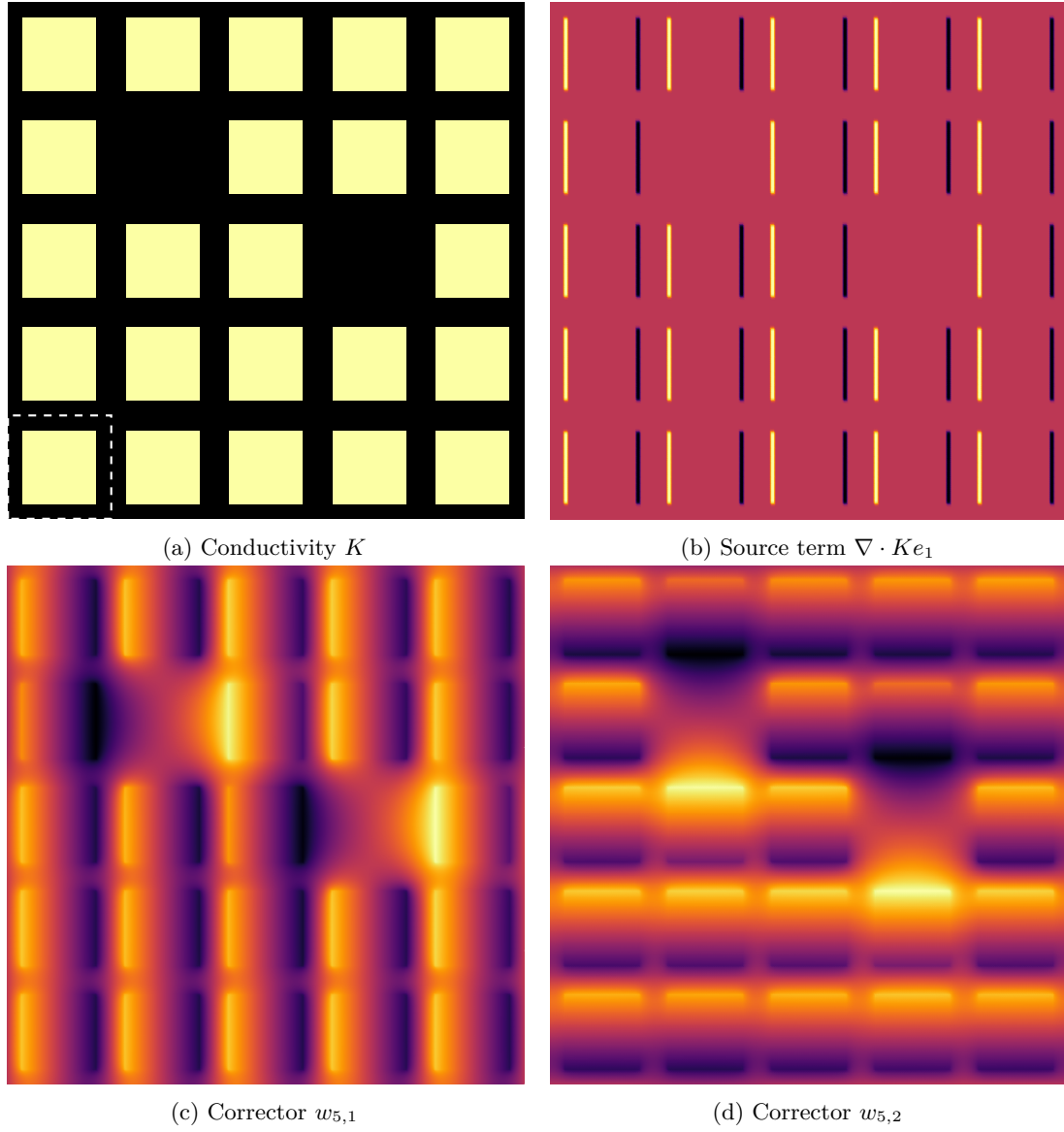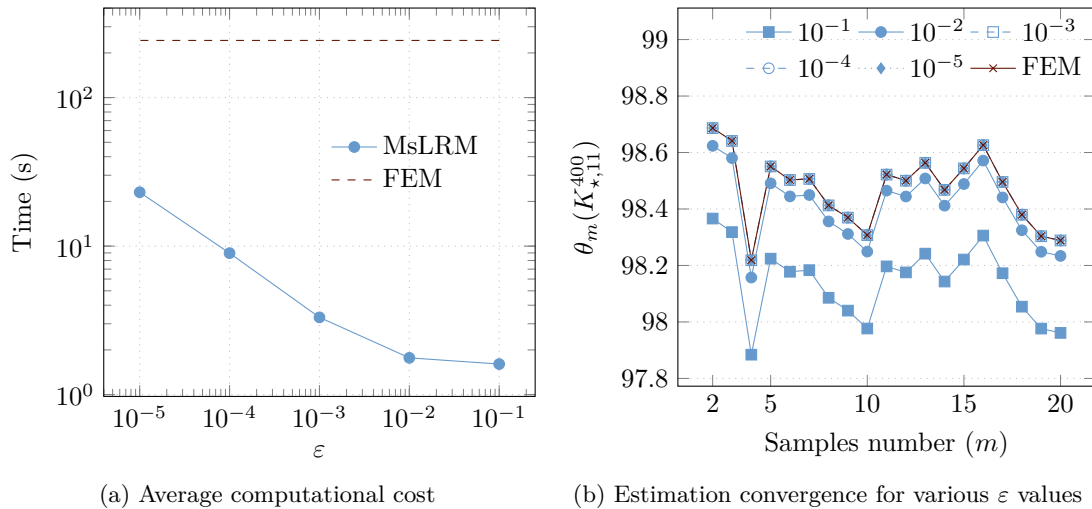[5]The same samples where used.

(a) Conductivity K

(b) Source term $\nabla \cdot K e_1$

(c) Corrector $w_{5,1}$

(d) Corrector $w_{5,2}$

Figure 4: Main test case (example for $N^2 = 25$)

(a) Average computational cost

(b) Estimation convergence for various ε values

Figure 5: MsLRM performance for various tolerances (20 samples; $N^2 = 400$)

computing the best approximation possible on the current modes library), hence the drawback of non-optimal low-rank approximation.

Nevertheless, this reduces significantly the time required by subsequent computations, as can be seen on table 2 from the average times and ranks, computed from all samples (not only the first 20). For comparison, the FEM time has been measured from a single computation. The average rank confirms that the modes library was complete with the first 6 modes.

Table 2: Comparison between FEM, MsLRM (with and without recycling)

	FEM	MsLRM	MsLRM+recycling
Average time per sample (s)	4040	5.76	3
Average rank per computation	–	6.15	6

3.2.3 Conductivity contrast

Here we evaluated the Monte Carlo estimator $\theta^\eta(K_\star^N)$ with the same samples for different values of K_2/K_1: 2, 10^1, 10^2, 10^3, 10^4 and 10^5. The number of samples required were computed with formula (2.12) with a variance estimated with 100 samples. It can be seen on figure 7b that this contrast affects greatly the estimator's variance, as expected. On the other hand, a high contrast seems to reduce the approximation cost (see figure 7a). One explanation is that the correctors' approximation is easier when the inter-phase peaks are so great that other variations become negligible. From now on, we will keep the conductivity contrast at 10^2 so that our medium remains significantly heterogeneous.

3.2.4 Defect probability

In a defect-type model such as described by equation (3.4), the defect probability p is an important characteristic of the random medium. That is one way to quantify periodicity loss. We computed an estimation $\theta^\eta(K_\star^N)$ for different values of p: 0.01, 0.1, 0.2, 0.3, 0.4 and 0.5.
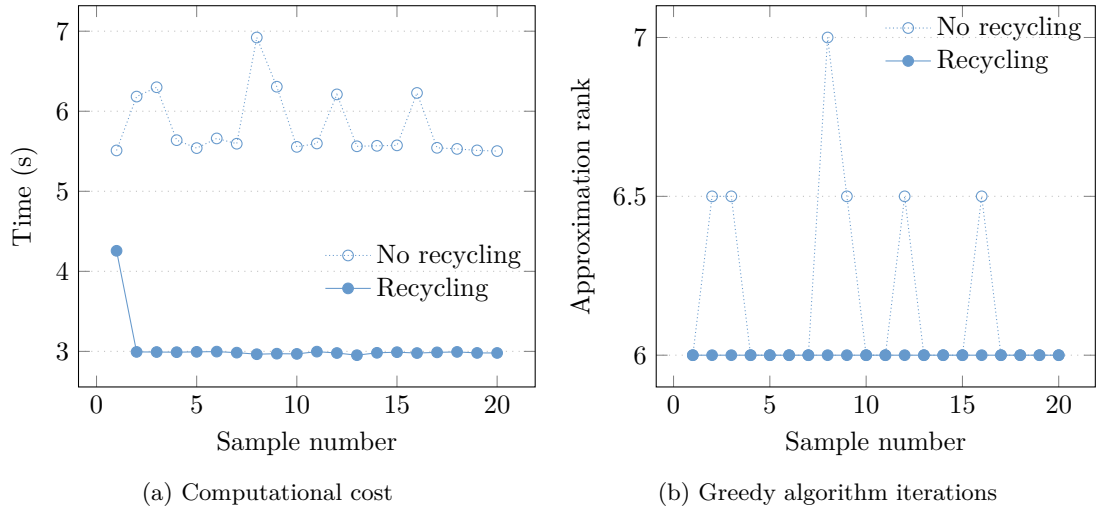
(a) Computational cost

(b) Greedy algorithm iterations

Figure 6: Modes recycling effect on MsLRM (averages across samples)

(a) Average computational cost

(b) Samples number required
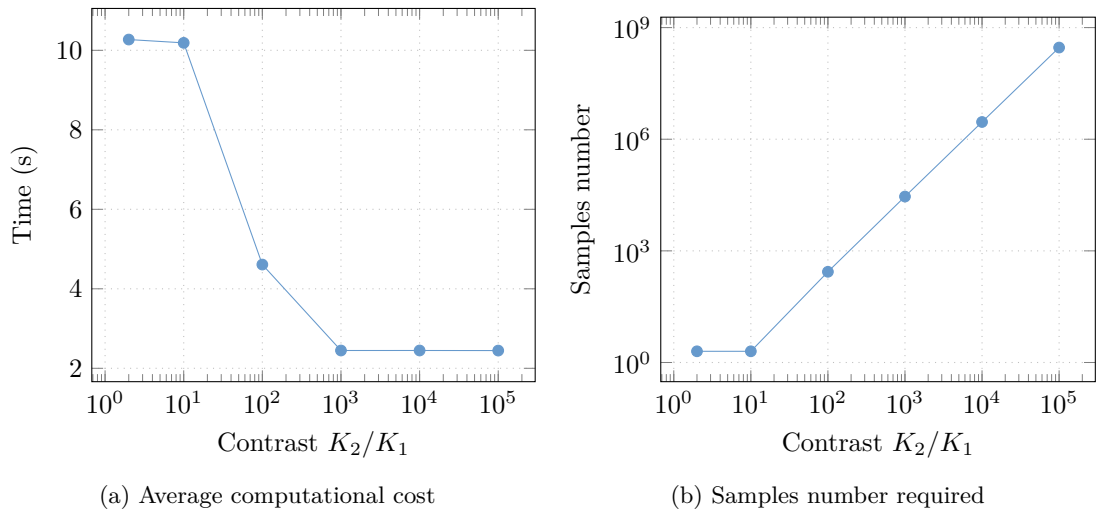
Figure 7: Conductivity contrast effect on MsLRM performance

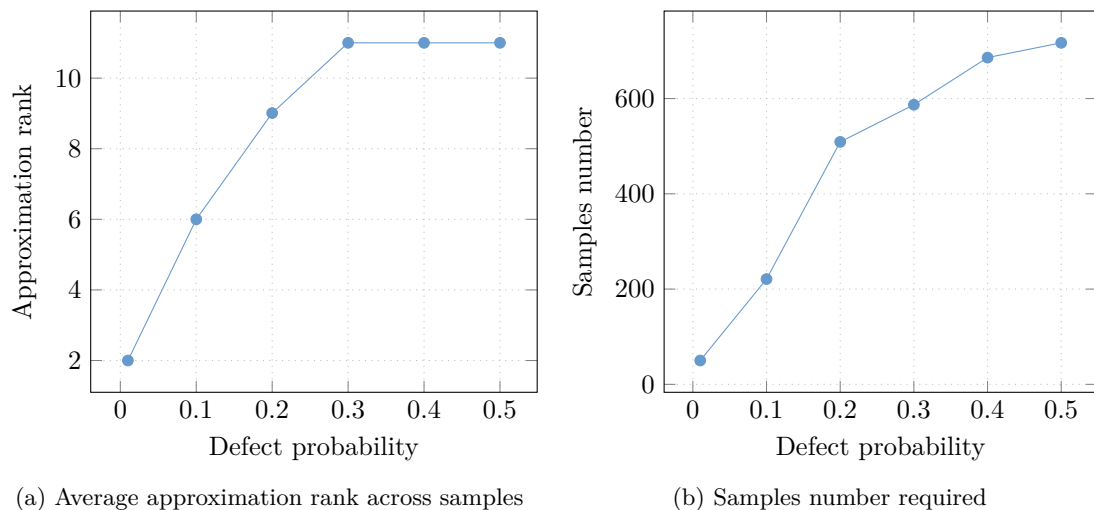(a) Average approximation rank across samples

(b) Samples number required

Figure 8: Defect probability effect on MsLRM performance

Figure 8a shows that the average approximation rank of correctors increases with p, as expected, until it reaches a plateau. Beyond a certain value of p (0.3 here), every configuration that would require new modes has become likely enough to occur, hence a rank plateau. We can relate this observation to the library completion previously discussed.

Figure 8b shows the impact of p on the estimator's variance (recalling the estimator's convergence rate (2.12)). We set p to 0.1 to keep the number of samples moderate.

3.2.5   Mesoscopic size

Recalling result (2.12), building an estimator with a good convergence rate is a compromise between domain size (which affects variance, see section 4) and number of samples. We showed a way to curb MsLRM computational cost increase with respect to sample number with modes recycling. However, an immediate advantage of MsLRM is its low sensitivity to domain size increase, even though modes recycling further reduces it. To illustrate this, we evaluated $\theta^\eta(K_\star^N)$ for several numbers of cells: 100, 400, 900, 1600, 2500 and 3600.

Additionally, we wish to broach the case of unidirectional periodicity. We dealt only with bi-directional periodicity so far, on square mesoscopic grids. Let us consider a unidirectional mesoscopic grid with reference cell $Y := [0,1] \times [0,10]$ so that a five-cells domain is $[0,5] \times [0,10]$ as illustrated on figure 9 (with Y outlined on figure 9a). We choose a conductivity $\hat{K}$ of the same form (3.4) but with χ replaced with $\hat{\chi}$ to get the patterns shown on figure 9a. This test case was inspired by unidirectional fibre-reinforced composite materials. We evaluate $\theta^\eta(\hat{K}_\star^N)$ as well, with the same values as above for the number of cells and the other parameters still set according to table 1.

First, we see on figure 10a the complexity reduction achieved, whatever the mesoscopic dimension. The MsLRM computational cost increase when the number of cells grows is moderate, particularly in comparison to the cost of the corresponding FEM solution[6] (displayed on the same graph, with identical values for both cases). Furthermore, figure 10b shows the rank's plateau caused by K's stationarity, as was discussed in subsection 3.1 on the topic of modes recycling.

---

[6]Measured from a single computation.

(a) Conductivity K (b) Source term $f = \nabla \cdot K e_1$ (c) Corrector w_1
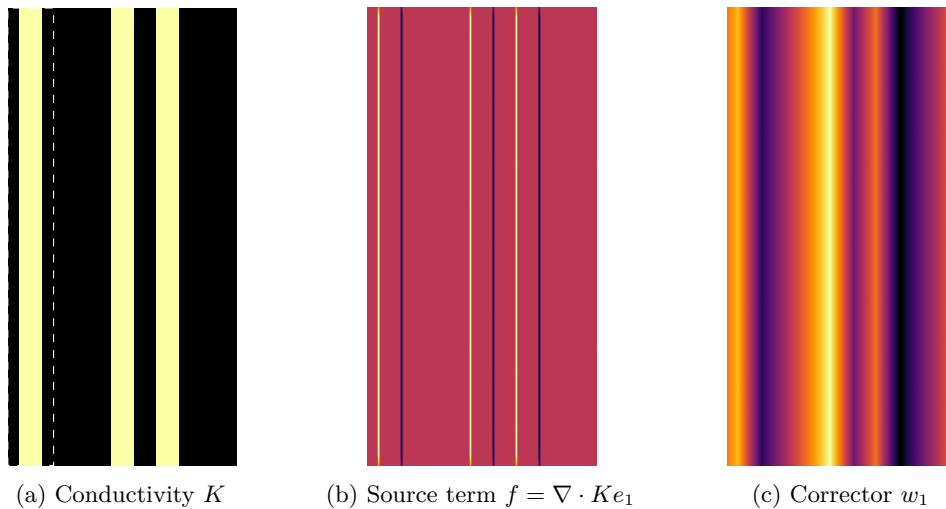
Figure 9: Unidirectional periodic medium (example with five cells)

Table 3: Domain size effect on samples number $m(\eta)$ and time required for estimation

#I	1D						2D					
	100	400	900	1600	2500	3600	100	400	900	1600	2500	3600
$m(\eta)$	4116	1107	467	229	164	106	4015	1089	457	227	163	105
Time (s)	6480	2012	1164	813	1030	1142	6552	1927	979	746	758	761

Secondly, it is clear from figure 10b that the complexity of the unidirectional case is considerably lower. A uni-dimensional grid brings the approximation's rank much closer to K's: any local loss of periodicity (faulty cell here) has much fewer neighbours to affect than in the previous case. The slight difference on figure 10a comes from a better conditioning of the bi-directional problem, due to homogeneity of K on cells boundaries.

As for the approximation in the bi-directional case, although it is almost constant the first point (100 cells) on figure 10b is worth commenting. We mentioned that the modes library is built in a non-optimal way; furthermore, it can only grow. Here, for every domain of 400 cells or more, the completion was almost immediate, i.e. the first sample was a good representation of the medium as far as the algorithm was concerned. With 100 cells, however, several samples had to be processed before reaching completion, each one causing some modes to be added to the library. These modes were the best choices for the sample, but not necessarily with regards to every possible realisation, hence a larger library.

Finally, table 3 shows how domain size affects the convergence rate of Monte Carlo estimation, as was mentioned above. Those values were estimated from 100 samples (as were all averages computed for this test case). For these estimators of identical variance η, the improved convergence rate somewhat balances the increase in computational time per sample in the overall cost of estimation, as the measured total times testify. Consequently, and although there is generally a compromise to be found to minimise the cost (more details in section 4), we observe a wide range of acceptable values for #I. The cost seems minimal around 1600 cells, so we chose this value as default (see table 1).

(a) Computational cost per sample
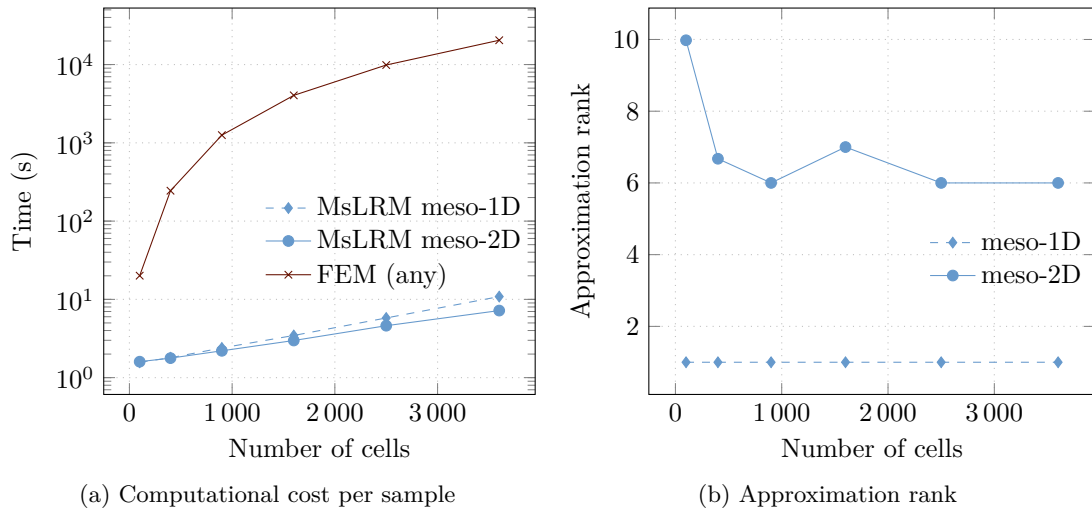
(b) Approximation rank

Figure 10: Domain size effect on MsLRM and FEM performance for uni- and bi-directional periodicity (averages across samples)

Table 4: Uniform laws' parameters

K_2^-	K_2^+	$(L_i)_{i \in \{1, \ldots, 10\}}$
1	100	$(i - 1) \times 0.1$

3.2.6   Aperiodic media with mesoscopic structure

In order to address a more general case where both the conductivity K_2 and the area it encompasses (represented by the characteristic function χ) may be random, we consider a broader variant of conductivity expression (3.4). For $(i, y, \omega) \in I \times Y \times \Omega$, we let

$$K(i, y, \omega) = K_1 + \chi_i(y, \omega)(K_{2,i}(\omega) - K_1),$$

where $K_{2,i}(\omega) \in \mathcal{U}([K_2^-, K_2^+])$ are independent and identically distributed, and each $\chi_i(\cdot, \omega) : Y \to \{0, 1\}$ is the characteristic function of the square of side length $\ell_i(\omega)$ centred relatively to the cell. The random variables $\ell_i \in \mathcal{U}(\{L_1, \ldots, L_q\}), i \in I$, are i.i.d. as well. An example is displayed on figure 11 and the chosen values for our tests are in table 4.

   We call such medium "aperiodic" because, for $i \neq j$, $\mathbb{P}(K(i, \cdot, \cdot) = K(j, \cdot, \cdot)) = 0$. Nevertheless, there is a spatial structure such that a mesoscopic grid can be defined, and we outlined the chosen reference cell Y on figure 11a. Here the rank r_K of K is a random variable whose values are bounded according to $(\ell_i)_{i \in I}$ probability laws: $r_K \leqslant 1 + q$ almost surely in this case. However, had we chosen $(\ell_i)_{i \in I}$ to be *continuous* random variables (e.g. $\ell_i \in \mathcal{U}([L_1, L_q])$), then $r_K = N^2$ almost surely.

   To get insight into the complexity of such problem, we perform the same tests as in subsection 3.2.5 (only the bi-directional case). The comparison of figures 10b and 12b reveals the increased complexity of the current case, and explains the difference between figures 10a and 12a; this was expected from the conductivities' rank difference: 2 against 10. Incidentally, this difference is due exclusively to the geometric variability introduced with (χ_i); indeed a rank-2 "aperiodic" conductivity (in the sense explained above) is possible. However, the FEM
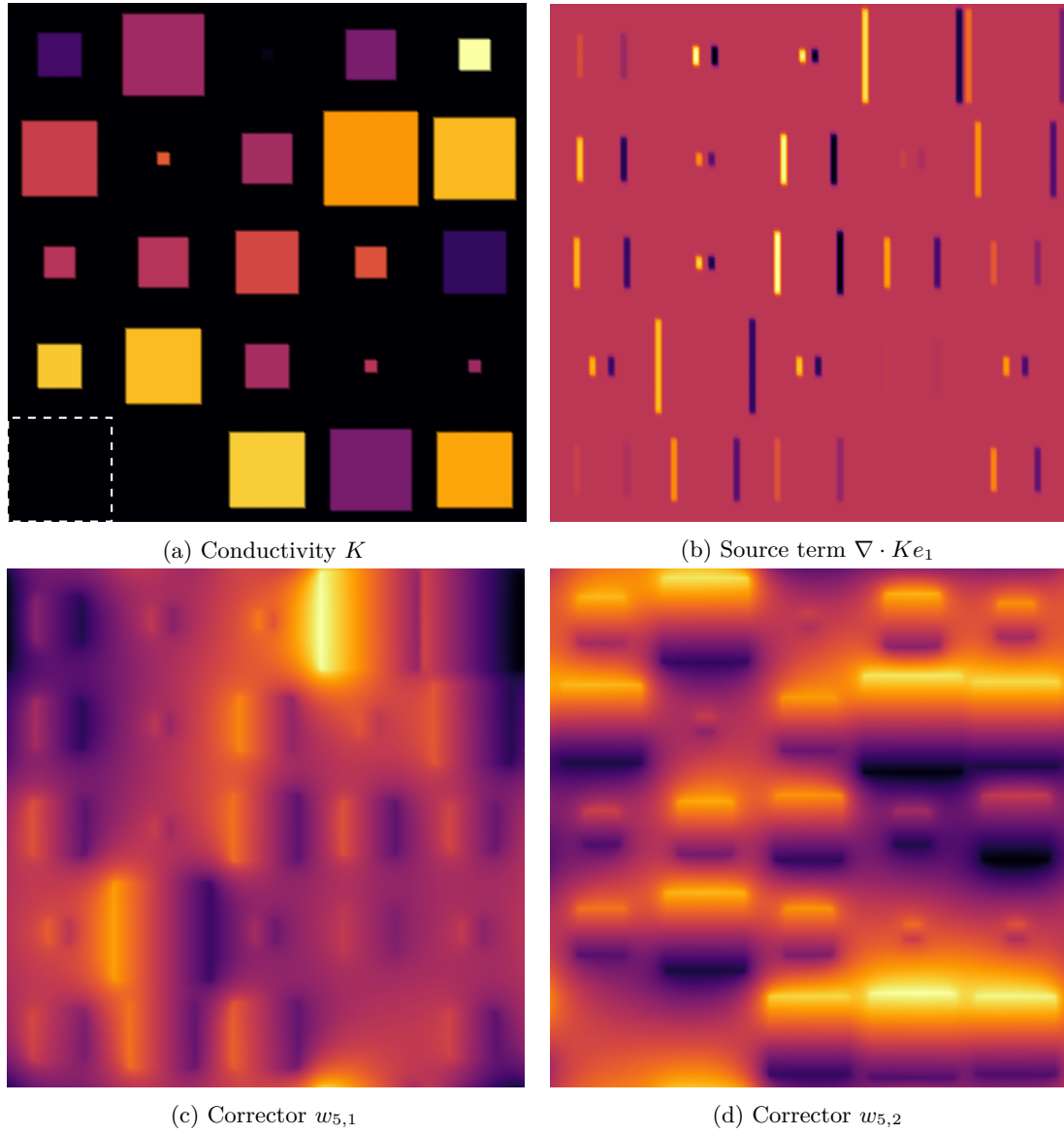
(a) Conductivity K

(b) Source term $\nabla \cdot Ke_1$

(c) Corrector $w_{5,1}$

(d) Corrector $w_{5,2}$

Figure 11: Aperiodic medium example for 25 cells

(a) Computational cost
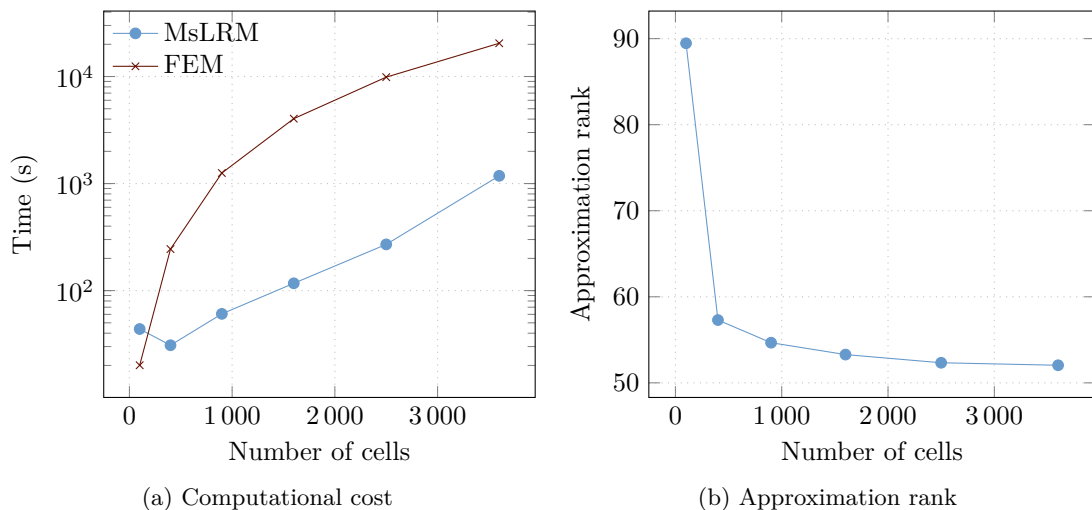

(b) Approximation rank

Figure 12: MsLRM performance on aperiodic medium (averages across samples)

Table 5: Sample number and time required on aperiodic medium

N^2	100	400	900	1600	2500	3600
$m(\eta)$	4627	961	510	297	191	124
Time (s)	202 530	29 637	30 889	34 707	51 475	145 960

computation times remind that the complexity reduction remains significant even in such aperiodic medium. As a side note, the computer reached its memory limit during MsLRM computations for $N^2 := 3600$, which somewhat diminished the performance.

Additionally, the increased rank of the approximations makes modes recycling particularly relevant here: the average values on figure 12 are based on 100 samples, and a greater number of samples would decrease the average time as the impact of the first computations' cost (from which the library was built) fades. To give more insight, the cost per sample on a complete library varied between 5 % and 17 % of the first sample's computation cost. Modes library was essentially completed within the first 8 samples, except the case $N^2 = 100$ which required around 35. The decreasing trend on figure 12b has the same explanation as was given in subsection 3.2.5, with greater variability in K.

Finally, we show on table 5 the number of samples required and associated total computation time (estimated from 100 samples). The comparison with table 3 shows how the increased computational cost has shifted the optimal cell number downward. In both tables, however, appears a minimal number of cells above which the total cost is of the same order of magnitude.

3.2.7 Transformed media

We illustrate here the use of MsLRM in the variant of stochastic homogenisation detailed in subsection 2.4. We define a periodic $K_\sharp = K_1 + \hat{\chi}(K_2 - K_1)$ with $\hat{\chi}$ introduced in subsection 3.2.5 for the unidirectional case (see figure 9) and choose a random diffeomorphism ϕ and let $K := K_\sharp \circ \phi^{-1}$. No fibre is missing this time, but the spaces between fibres are independent random variables $(\ell_i)_{i \in \{0,\dots,\#I\}}$ following the same uniform law $\mathcal{U}([0.1, 2])$. The two limit fibres in D_1 and $D_{\#I}$ are

separated from the domain boundary by respectively $\ell_0/2$ and $\ell_{\#I}/2$ and the fibre width is a constant denoted δ. The chosen random diffeomorphism ϕ is then continuous, piecewise affine and expressed component-wise $\phi(i, y) = \phi_1(i, y)e_1 + (\zeta(i, y) \cdot e_2)e_2$. Therefore, nothing is changed along e_2 and ϕ_1 has the rank-4 representation $\phi_1 = \phi_0^I \otimes 1^Y + \phi_1^I \otimes \phi_1^Y + 1^I \otimes \phi_2^Y + \phi_3^I \otimes \phi_3^Y$, where

$$\phi_0^I(i) = \begin{cases} 0 & \text{if } i = 1 \\ \dfrac{\ell_0}{2} + \dfrac{\ell_{i-1}}{2} + (i-1)\delta + \displaystyle\sum_{k=1}^{i-2} \ell_k & \text{else} \end{cases} \, , \; \phi_1^I(i) = \frac{\ell_{i-1}}{1-\delta}, \; \phi_3^I(i) = \frac{\ell_i}{1-\delta},$$

and

$$\phi_1^Y(y) = \min\left(y_1, \frac{1-\delta}{2}\right), \; \phi_2^Y(y) = \max\left(0, \min\left(\delta, y_1 - \frac{1-\delta}{2}\right)\right),$$

$$\phi_3^Y(y) = \max\left(0, y_1 - \frac{1+\delta}{2}\right).$$

We noted 1^I and 1^Y the constant functions of value 1 and $y_1 := y \cdot e_1$. This gradient of this transformation is expressed

$$\nabla \phi = \begin{pmatrix} \phi_{1,1} & 0 \\ 0 & 1^I \otimes 1^Y \end{pmatrix} \quad \text{with } \phi_{n,1} = \frac{\partial \phi_n}{\partial x_1},$$

so $\det(\nabla \phi) = \phi_{1,1} = \phi_1^I \otimes \phi_{1,1}^Y + 1^I \otimes \phi_{2,1}^Y + \phi_3^I \otimes \phi_{3,1}^Y$. Here $\nabla(\phi^{-1}) = (\nabla \phi)^{-1}$ thus the ensuing simplifications in $\tilde{K} := \det(\nabla \phi) \nabla \phi^{-1} K_\sharp {}^t\nabla \phi^{-1}$ yield $\operatorname{rank}(\tilde{K}) = 3$. The effects of this transformation are illustrated on figure 13 with an example of realisation of K and its associated source term and first corrector function.

In this test, we solve the corrector problems (2.15). We perform the same tests as for the unidirectional case in subsection 3.2.5. The performance, shown on figure 14, is between that on figure 10 and that on figure 12, which suggests that these tests are comparable enough for the performance to be dominated by r_K's influence. This is a consequence of the correctors problems' nature: the source term follows the same quasi-periodicity as K, and boundary conditions do not break this quasi-periodicity in the solution. Therefore, the only periodicity loss in the solution comes from K.

(a) Conductivity K (b) Source term $f = \nabla \cdot (Ke_1)$ (c) Corrector $w_{5,1}$
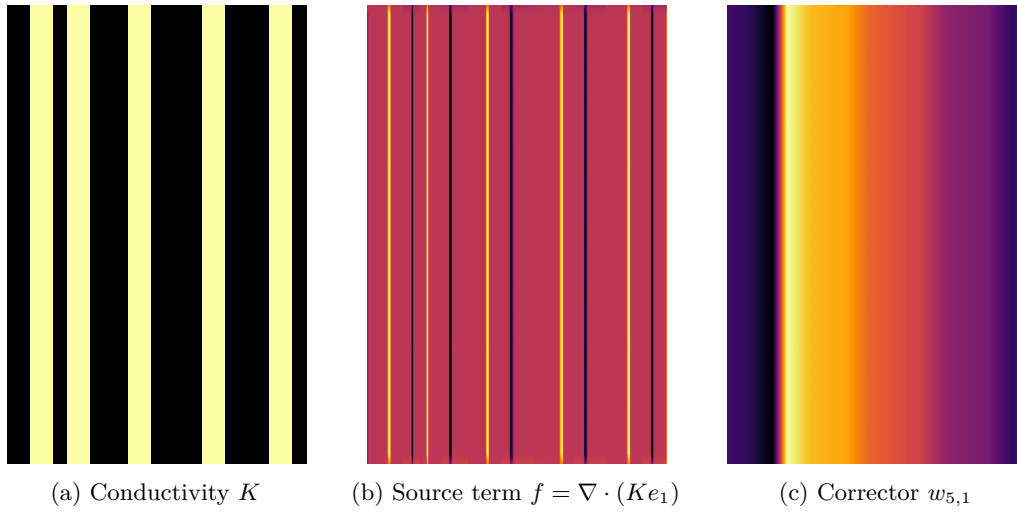
Figure 13: Example of randomly transformed medium for 5 cells.

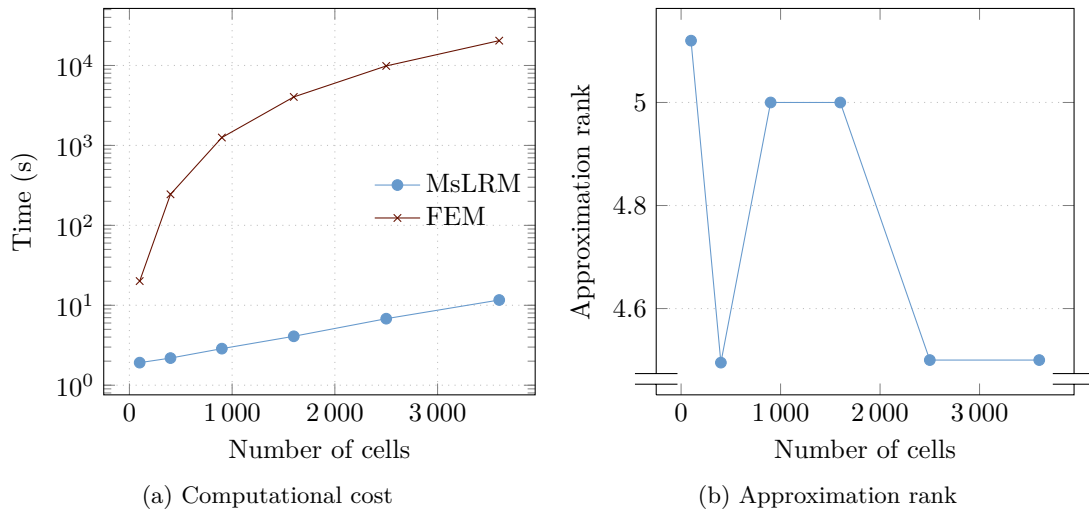(a) Computational cost   (b) Approximation rank

Figure 14: MsLRM performance on transformed medium (averages across samples)

4 Variance reduction by control variate

The error associated with approximation of $K_\star$ by $\theta_m(K_\star^N)$ (from (2.11)) can be decomposed as

$$K_\star - \theta_m(K_\star^N) = \underbrace{K_\star - \mathbb{E}(K_\star^N)}_{\textbf{systematic } \text{error}} + \underbrace{\mathbb{E}(K_\star^N) - \theta_m(K_\star^N)}_{\textbf{statistical } \text{error}}.$$

It has been proven that

$$\mathbb{E}(K_\star - \mathbb{E}(K_\star^N)) \lesssim N^{-d}\ln^d(N) \quad [\text{in } 17]$$

$$\text{and} \quad \sqrt{\mathbb{E}((\mathbb{E}(K_\star^N) - \theta_m(K_\star^N))^2)} \lesssim (N^d m)^{-1/2} \quad [\text{in } 18, 19]$$

for a cubic domain of side length proportional to N. Consequently, the bias decreases fast with domain size and the statistical error is usually the major contribution to the error. As was mentioned in equation (2.12), this statistical error can be quantified as

$$\mathbb{E}\left(\left(\theta_m(\tilde{X}) - \mathbb{E}(\tilde{X})\right)^2\right) = \mathbb{V}\text{ar}\left(\theta_m(\tilde{X})\right) = \frac{\mathbb{V}\text{ar}(\tilde{X})}{m}$$

for any random variable $\tilde{X} \in L^2(\Omega)$, hence the numerous variance reduction techniques developed to accelerate Monte Carlo method's convergence rate. Such techniques include stratified sampling, importance sampling, antithetic variates, control variates and many more; we are interested in the latter.

Let $\rho \in \mathbb{R}$ and let $Z \in L^2(\Omega)$ be a random variable. Z serves as a control variate by defining the controlled variable $X = \tilde{X} - \rho(Z - \mathbb{E}(Z))$. We have, purposely, $\mathbb{E}(\tilde{X}) = \mathbb{E}(X)$. As for the variance, $\mathbb{V}\text{ar}(X) = \mathbb{V}\text{ar}(\tilde{X}) - 2\rho\,\mathbb{C}\text{ov}(\tilde{X}, Z) + \rho^2\,\mathbb{V}\text{ar}(Z)$ and is minimal for

$$\rho = \frac{\mathbb{C}\text{ov}(\tilde{X}, Z)}{\mathbb{V}\text{ar}(Z)}, \tag{4.1}$$

with minimum

$$\min_{\rho \in \mathbb{R}} \mathbb{V}\text{ar}(X) = \left(1 - \frac{(\mathbb{C}\text{ov}(\tilde{X}, Z))^2}{\mathbb{V}\text{ar}(\tilde{X})\,\mathbb{V}\text{ar}(Z)}\right)\mathbb{V}\text{ar}(\tilde{X}). \tag{4.2}$$

We observe from equation (4.2) that, whatever Z, a variance reduction can be achieved with a suitable parameter ρ. A good control variate would be closely correlated to $\tilde{X}$: the higher the correlation between $\tilde{X}$ and Z, the greater the variance reduction. However, $\mathbb{E}(Z)$ must be precisely known lest the control variate introduces a bias. Additionally, the benefit of an optimal ρ comes at the cost of estimating $\mathbb{V}\text{ar}(Z)$ and $\mathbb{C}\text{ov}(\tilde{X}, Z)$.

What we actually do is estimate $\mathbb{E}(X) = \mathbb{E}(U) + \rho\mathbb{E}(Z)$, with $U := \tilde{X} - \rho Z$, as

$$\theta_{n_U, n_Z}(X) = \frac{1}{n_U}\sum_{k=1}^{n_U} U(\omega_k) + \frac{\rho}{n_Z}\sum_{k=1}^{n_Z} Z(\omega_k') \tag{4.3}$$

where ω and ω' are i.i.d. samples, with variance

$$\mathbb{V}\text{ar}(\theta_{n_U, n_Z}(X)) = \frac{\mathbb{V}\text{ar}(U)}{n_U} + \frac{\rho^2\,\mathbb{V}\text{ar}(Z)}{n_Z}. \tag{4.4}$$

This estimation's cost is $c_{n_U, n_Z} = n_U c_U + n_Z c_Z$ with $c_U := c_0 + c_Z$, where $c_0 := \text{cost}(\tilde{X})$ and $c_Z := \text{cost}(Z)$ denote the cost of an evaluation of $\tilde{X}$ and Z, respectively. For a given variance η^2, we minimise c_{n_U, n_Z} over $(n_U, n_Z) \in \mathbb{R}^2$ by solving the equivalent saddle-point problem

$$\max_{\lambda \geqslant 0} \min_{n_U, n_Z \geqslant 0} c_u n_u + c_Z n_Z + \lambda \left(\frac{\mathbb{V}\text{ar}(U)}{n_U} + \frac{\rho^2 \, \mathbb{V}\text{ar}(Z)}{n_Z} - \eta^2 \right),$$

which yields $n_U \sqrt{c_U \rho^2 \, \mathbb{V}\text{ar}(Z)} = n_Z \sqrt{c_Z \, \mathbb{V}\text{ar}(U)}$. Therefore, equation (4.4) now reads

$$\mathbb{V}\text{ar}(\theta_{n_U, n_Z}(X)) = \frac{1}{n_Z} \left(\rho^2 \, \mathbb{V}\text{ar}(Z) + \sqrt{\mathbb{V}\text{ar}(U) \, \mathbb{V}\text{ar}(Z) \rho^2 \frac{c_U}{c_Z}} \right)$$

with

$$n_Z = \left\lceil \frac{1}{\eta^2} \left(\rho^2 \, \mathbb{V}\text{ar}(Z) + \sqrt{\mathbb{V}\text{ar}(U) \, \mathbb{V}\text{ar}(Z) \rho^2 \frac{c_U}{c_Z}} \right) \right\rceil \text{ and } n_U = \left\lceil n_Z \sqrt{\frac{c_Z \, \mathbb{V}\text{ar}(U)}{c_U \, \mathbb{V}\text{ar}(Z) \rho^2}} \right\rceil \quad (4.5)$$

for a variance of[7] η^2. Like expectations, variances and covariances are estimated empirically. For two random variables A and B, with a sample $(\omega_i)_{i \in \{1, \dots, m\}}$ of size $m \in \mathbb{N}_*$, we define

$$\varsigma_m(A, B) := \frac{1}{m-1} \sum_{i=1}^{m} (A(\omega_i) - \theta_m(A))(B(\omega_i) - \theta_m(B)).$$

This is an unbiased estimator, i.e. $\mathbb{C}\text{ov}(A, B) = \mathbb{E}(\varsigma_m(A, B))$; obviously, $\mathbb{V}\text{ar}(A) = \mathbb{E}(\varsigma_m(A, A))$. We set a minimal sample size required to get a reliable estimation of $\mathbb{V}\text{ar}(U)$, $\mathbb{V}\text{ar}(Z)$, c_U and c_Z before estimating n_Z and n_U. Likewise, the optimal control coefficient value is estimated from formula (4.1) as $\varsigma_{n_U}(\tilde{X}, Z) / \varsigma_{\max(n_U, n_Z)}(Z)$.

A cost-efficient approximation of the homogenised operator, provided by a surrogate model, would be a closely correlated random variable. In a situation where the surrogate model does not provide a satisfying approximation, it remains a suitable control variate Z to a more precise, and costlier, solution $\tilde{X}$. We will first present a control variate that has been introduced a few years ago in a similar context of quasi-periodicity by Legoll and Minvielle [22], then propose another one based on the tensor-based approximation method.

4.1   Weakly stochastic approach

4.1.1   Defect-type surrogate model

The various surrogate models of weakly stochastic homogenisation have been set in the theoretical framework outlined in subsections 2.3 and 2.4 and address randomly perturbed periodic media. They all rely on an asymptotic development of corrector functions with respect to a parameter which quantifies the weakness of the perturbation, hence the name. Different surrogate models have been proposed for different perturbation's modelling [as in 2, 8, 34], and we are interested in one proposed for the specific context of local material defects at the microscopic scale. This "defect-type" approach, introduced by Anantharaman and Le Bris [3], is based on the assumptions that every material cell[8] is either sound or faulty (all defects being identical), that every cell has the same probability ϵ of being faulty and that this probability is small.

---

[7] The variance is actually slightly lower, due to the ceil function $\lceil \cdot \rceil$.
[8] Period of the reference unperturbed material.

Proposition 4 (Defect-type perturbation). *Let $K \in \mathcal{M}(\alpha, \beta)$ be such that*

$$K(x, \omega) = K_\sharp(x) + K_{def}(x) \sum_{i \in I} \mathbb{1}_{D_i}(x) B_\epsilon^i(\omega), \quad \forall (x, \omega) \in \mathbb{R}^d \times \Omega,$$

with $K_\sharp$ and K_{def} periodic, and independent random variables $\left(B_\epsilon^i\right)_{i \in I}$ following the Bernoulli law of parameter ϵ, so that $\mathbb{P}(B_\epsilon^i = 1) = \epsilon$. Then,

$$K_\star = \lim_{N \to \infty} K_{\sharp\star} + \epsilon N^d K_{1\star}^N + \epsilon^2 K_{2\star}^N + o(\epsilon^2)$$

where $K_{\sharp\star}$ is the periodic homogenised operator defined in proposition 1,

$$\left(K_{1\star}^N\right)_{ij} := \frac{1}{|D|} \int_D (e_i + \nabla w_i^{1,N}) \cdot (K_\sharp + \mathbb{1}_{D_1} K_{def}) \cdot e_j - (K_{\sharp\star})_{ij},$$

with the d correctors $w_i^{1,N} \in H_\sharp^1(D)$ solutions of

$$-\nabla \cdot \left((K_\sharp + \mathbb{1}_{D_1} K_{def}) \cdot (e_i + \nabla w_i^{1,N}) \right) = 0,$$

and

$$K_{2\star}^N = \frac{1}{2} \sum_{l \in I} \sum_{m \in I \setminus \{l\}} K_{2\star}^{1+|m-l|,N} \tag{4.6}$$

where

$$\left(K_{2\star}^{k,N}\right)_{ij} = \frac{1}{|D|} \int_D \left(e_i + \nabla w_{i,k}^{2,N} \right) \cdot (K_\sharp + \mathbb{1}_{D_1 \cup D_k} K_{def}) \cdot e_j - 2\left(K_{1\star}^N\right)_{ij} + (K_{\sharp\star})_{ij},$$

with the $d \times (N^d - 1)$ correctors $w_{i,k}^{2,N} \in H_\sharp^1(D)$ solutions of

$$-\nabla \cdot \left((K_\sharp + \mathbb{1}_{D_1 \cup D_k} K_{def}) \left(e_i + \nabla w_{i,k}^{2,N} \right) \right) = 0.$$

Proof. See Anantharaman and Le Bris [4]. $\qquad\square$

In proposition 4, sound cells have diffusion coefficient $K_\sharp$ and faulty cells have $K_\sharp + K_{def}$. As an example, the conductivity expressed in (3.4), involved in most tests of subsection 3.2, falls in this defect-type category. As in subsection 3.2, we still consider isotropic mesoscopic grids of N cells along each direction so $\#I = N^d$, and set as reference cell $Y := D_1$, the "first" cell.

The terms $K_{1\star}^N$ and $K_{2\star}^{k,N}$ are referred to as 1-defect and 2-defects individual contributions, respectively. They are the homogenised operators associated with the periodic repetition of domain D with, respectively, one and two defects. Due to periodicity, only the relative localisation of one defect with respect to the other affects the apparent homogenised operator; with only one defect, its position does not matter. Therefore, the total 1-defect contribution is $N^d K_{1\star}^N$ whereas the total 2-defects contribution is defined by equation (4.6), where we chose arbitrarily to place the first defect in D_1. The "0-defect" contribution is, obviously, $K_{\sharp\star}$.

4.1.2 Variance reduction based on defect-type model

Weakly stochastic homogenisation provides a surrogate model whose accuracy is related to perturbation weakness. When the perturbation is not weak enough for that model to provide the desired accuracy, its approximation remains supposedly highly correlated to the estimated homogenised operator $K_\star^N$. Therefore, it can be used as control variate in the Monte Carlo estimation $\theta_m(K_\star^N)$ (from equation (2.11)), as detailed in the introduction of section 4, where $K_\star^N$ is evaluated by FEM. This variance reduction scheme has been published by Legoll and Minvielle [in 22] for the defect-type approach from proposition 4. We will outline the method here and refer the reader to this publication for a detailed explanation and justification of what follows.

Proposition 4 offers a second-order approximation from which can be deduced either a first- or second-order controlled variable, depending on whether the second-order term is accounted for. This decision is a compromise between accuracy and cost-efficiency, which will be discussed in subsection 4.3. The first-order controlled variable is defined as

$$X_1 = K_\star^N - \rho_1(Z_1 - \mathbb{E}(Z_1))$$

with

$$Z_1 = K_{\sharp\star} + \sum_{i \in I} B_i^\epsilon K_{1\star}^N, \quad \text{and} \quad \mathbb{E}(Z_1) = K_{\sharp\star} + \epsilon N^d K_{1\star}^N,$$

therefore, our first-order controlled variable reads

$$X_1 = K_\star^N - \rho_1 \left(\sum_{i \in I} B_i^\epsilon - \epsilon N^d \right) K_{1\star}^N$$

and, from (4.1), the optimal control coefficient value is

$$\rho_1 = \frac{\mathbb{C}\text{ov}(K_\star^N, Z_1)}{\mathbb{V}\text{ar}(Z_1)}.$$

We used here the same notations as in proposition 4. Henceforth we will note $c_N := \text{cost}(K_\star^N)$ and, accordingly, $c_1 := \text{cost}(K_{\sharp*})$. The computational cost related to control variate Z_1 can be broken down into an a priori cost c_{p1} and the cost of evaluating a new realisation of Z_1. The latter is deemed negligible[9] while former amounts to the computation of $K_{\sharp\star}$ and $K_{1\star}^N$, hence $c_{p1} := c_{FE} + c_1$.

The second-order controlled variable is expressed as

$$X_2 = K_\star^N - \rho_1(Z_1 - \mathbb{E}(Z_1)) - \rho_2(Z_2 - \mathbb{E}(Z_2)) - \check{\rho}_2\left(\check{Z}_2 - \mathbb{E}\left(\check{Z}_2\right)\right)$$

with

$$Z_2 = \frac{1}{2} \sum_{i \in I} \sum_{j \in I \setminus \{i\}} B_i^\epsilon B_j^\epsilon K_{2\star}^{1+|j-i|,N} \quad \text{so } \mathbb{E}(Z_2) = \frac{\epsilon^2}{2} \sum_{i \in I} \sum_{j \in I \setminus \{i\}} K_{2\star}^{1+|j-i|,N},$$

and

$$\check{Z}_2 = \frac{1}{2} \sum_{i \in I} \sum_{j \in I \setminus \{i\}} (1 - B_i^\epsilon)(1 - B_j^\epsilon), \check{K}_{2\star}^{1+|j-i|,N} \quad \text{so } \mathbb{E}\left(\check{Z}_2\right) = \frac{(1-\epsilon)^2}{2} \sum_{i \in I} \sum_{j \in I \setminus \{i\}} \check{K}_{2\star}^{1+|j-i|,N}.$$

---

[9]Compared to, e.g. c_1.

We introduced above the quantity $\check{K}_{2\star}^{k,N}$ for $k \in I$. It is the counterpart of $K_{2\star}^{k,N}$ for the "complementary" material, i.e. the material whose reference conductivity is $K_\sharp + K_{def}$ and whose faulty cells have conductivity $K_\sharp$. Consequently, the associated 2-defects individual contributions are

$$\left(\check{K}_{2\star}^{k,N}\right)_{ij} := \frac{1}{|D|} \int_D (e_i + \nabla \check{w}_{i,k}^{2,N}) \cdot (K_\sharp + K_{def} - \mathbb{1}_{D_1 \cup D_k} K_{def}) \cdot e_j - 2\check{K}_{1\star}^N + \check{K}_{\sharp\star}$$

$$\text{with} \quad -\nabla \cdot \left((K_\sharp + K_{def} - \mathbb{1}_{D_1 \cup D_k} K_{def})(e_i + \nabla \check{w}_{i,k}^{2,N})\right) = 0,$$

and the 1-defect individual contribution is

$$\left(\check{K}_{1\star}^N\right)_{ij} := \frac{1}{|D|} \int_D (e_i + \nabla \check{w}_i^{1,N}) \cdot (K_\sharp + K_{def} - \mathbb{1}_{D_1} K_{def}) \cdot e_j - (\check{K}_{\sharp\star})_{ij}$$

$$\text{with} \quad -\nabla \cdot \left((K_\sharp + K_{def} - \mathbb{1}_{D_1} K_{def}) \cdot (e_i + \nabla \check{w}_i^{1,N})\right) = 0,$$

and, finally, the periodically homogenised operator is

$$(\check{K}_{\sharp\star})_{ij} := \frac{1}{|Y|} \int_Y (e_i + \nabla \check{w}_i^\sharp) \cdot (K_\sharp + K_{def}) e_j,$$

$$\text{with} \quad -\nabla \cdot \left((K_\sharp + K_{def})(e_i + \nabla \check{w}_i^\sharp)\right) = 0.$$

This additional contribution was ignored in proposition 4 because we assumed $\epsilon \ll 1$. There is no such assumption here and therefore no precedence of one reference over the other. This does not apply at the first order, for which considering one or the other is equivalent. Indeed, the first-order control variate accounts only for the proportion of faulty cells without geometric consideration.

As for the control coefficients ρ_1, ρ_2 and $\check{\rho}_2$, their optimal values are solutions to

$$\begin{pmatrix} \mathbb{V}\mathrm{ar}(Z_1) & \mathbb{C}\mathrm{ov}(Z_1, Z_2) & \mathbb{C}\mathrm{ov}(Z_1, \check{Z}_2) \\ \mathbb{C}\mathrm{ov}(Z_2, Z_1) & \mathbb{V}\mathrm{ar}(Z_2) & \mathbb{C}\mathrm{ov}(Z_2, \check{Z}_2) \\ \mathbb{C}\mathrm{ov}(\check{Z}_2, Z_1) & \mathbb{C}\mathrm{ov}(\check{Z}_2, Z_2) & \mathbb{V}\mathrm{ar}(\check{Z}_2) \end{pmatrix} \begin{pmatrix} \rho_1 \\ \rho_2 \\ \check{\rho}_2 \end{pmatrix} = \begin{pmatrix} \mathbb{C}\mathrm{ov}(K_\star^N, Z_1) \\ \mathbb{C}\mathrm{ov}(K_\star^N, Z_2) \\ \mathbb{C}\mathrm{ov}(K_\star^N, \check{Z}_2) \end{pmatrix}. \tag{4.7}$$

The a priori cost c_{p2} of this second-order control variate is significantly higher than the first-order one: $c_{p2} = 2(C_1 + (N^d - 1)C_{FE})$. The subsequent cost of every realisation is admittedly higher as well, mainly due to the resolution of (4.7), yet we still deem it negligible.

Obviously, the cost of these a priori computations could be greatly reduced by MsLRM. Even more so because modes recycling would be most efficient in this case.

4.2 Low-rank approximation as control variate

Results from subsection 3.2 hinted at the MsLRM limits, i.e. situations where a more general and simple direct resolution (e.g. FEM) would be more efficient. These situations occur mostly when the rank required to achieve the desired precision is too high, because either the tolerance is too low or the quasi-periodicity too weak. To address these situations, we wish to propose a MsLRM-based low-fidelity model as a control variate to $K_\star^N$ evaluated by a high-fidelity model— FEM here. First, we observed that the rank of K had a significant effect on the approximation's rank. To address cases where K may not be quasi-periodic, one way to provide a cost-efficient approximation would be to use a low-rank approximation of K. However, to guarantee the approximation's quality we must still be able to control the precision of this perturbed MsLRM.

Let $\varepsilon \in \mathbb{R}_{+*}$, we note U_i^ε the function from $\mathcal{M}(\alpha, \beta)$ to $V_h(D)$ which maps K to the MsLRM approximation $w_{N,i}^\varepsilon$ of the apparent corrector solution to (2.9) (for a chosen $i \in \{1, \dots, d\}$). We choose $\delta \in \mathbb{R}_{+*}$ and let $\tilde{K} \in L^\infty(D)$ be such that $\|\tilde{K} - K\|_{L^\infty(D)} \leqslant \delta$ and $\mathrm{rank}(\tilde{K})$ is low. Then, assuming $U_i^\varepsilon \in C^0(L^\infty(D); V_h(D))$, we have $\|U_i^\varepsilon(\tilde{K}) - U_i^\varepsilon(K)\| \leqslant C_U \delta$ where C_U denotes the Lipschitz constant of U_i^ε. Consequently, we can control the error caused on the MsLRM approximation by the approximation on K, provided that we can control δ.

Then, let us note $Z_{\delta,\varepsilon}$ the function from $L^2(\Omega; \mathcal{M}(\alpha, \beta))$ to $L^2(\Omega; L^\infty(D)^{d \times d})$ which maps K to the apparent homogenised operator associated to $\tilde{K}$ with MsLRM approximation to the precision ε of the correctors, i.e.

$$(Z_{\delta,\varepsilon}(K))_{ij} := \frac{1}{|D|} \int_D e_i \cdot \tilde{K}(e_j + \nabla U_j^\varepsilon(\tilde{K})). \tag{4.8}$$

We hope to provide a cost-efficient, highly correlated control variate $Z_{\delta,\varepsilon}(K)$ to $K_\star^N$. More precisely, we hope to achieve cost-efficiency for aperiodic conductivities K with large enough δ and ε while remaining highly correlated to $K_\star^N$. We note the controlled variable

$$X_{\delta,\varepsilon} := K_\star^N + \rho(Z_{\delta,\varepsilon} - \mathbb{E}(Z_{\delta,\varepsilon})),$$

where control coefficient ρ is computed according to expression (4.1). The process that yield $X_{\delta,\varepsilon}$ from K^N is summarised on figure 15.
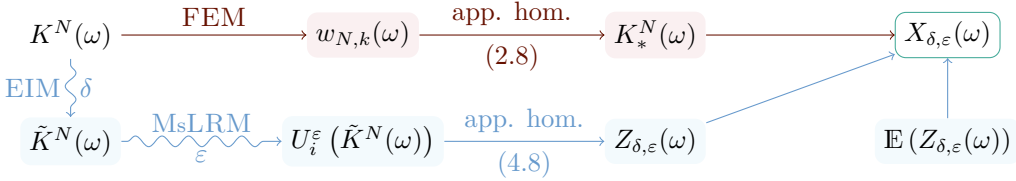

Figure 15: Combination of high- and low-fidelity models into controlled variable $X_{\delta,\varepsilon}$

The low-rank approximation $\tilde{K}$ is built as an empirical interpolation of K in the form $\mathcal{I}_n[K] := \sum_{j=1}^n \alpha_j^n \otimes q_j$ by greedy algorithm 1. At every step $n \in \mathbb{N}_*$, the interpolation points (i_n, y_n) are defined to be where the current interpolation is worse. Then q_n is chosen colinear to $K(i_n, \cdot) - \mathcal{I}_{n-1}[K](i_n, \cdot)$ and such that $q_n(y_n) = 1$. Since the matrix $(q_j(y_p))_{(j,p) \in \{1, \dots, n\}^2}$ is invertible[10], we can choose α_n such that $\forall (i, p) \in I \times \{1, \dots, n\}, \mathcal{I}_n[K](i, y_p) = K(i, y_p)$. Once $\|K - \mathcal{I}_n[K]\|_{L^\infty(D)} \leqslant \delta$, we stop and keep approximation $\tilde{K} := \mathcal{I}_n[K]$. The a priori error estimation $\max_{i \in I} \|K(i, \cdot) - \mathcal{I}_n[K](i, \cdot)\|_{L^\infty(Y)} \leqslant (1 + \Lambda_n) \inf_{\kappa \in \mathcal{K}_n} \|K - \kappa\|_{L^\infty(Y)}$ holds, with $\mathcal{K}_n := \mathrm{span}\{\{K(i_p, \cdot), p \in \{1, \dots, n\}\}\}$ and the Lebesgue constant $\Lambda_n := \sup_{y \in Y} \sum_{j=1}^n |h_j^n(y)| \leqslant 2^n - 1$, where $h_j^n \in \mathcal{K}_n$ is such that $\forall p \in \{1, \dots, n\}, h_j^n(y_p) = \delta_{jp}$. From the quasi-periodicity assumption on K, we expect $\inf_{\kappa \in \mathcal{K}_n} \|K - \kappa\|_{L^\infty(Y)}$ to decrease rapidly with n and thus believe that algorithm 1 can provide accurate and low-rank approximations in our case. For a detailed explanation of the Empirical Interpolation Method (EIM), we refer the reader to [6, 24].

Remark 3 (Multi-level control variates). The benefit of a control variate to an estimator is measured by the error reduction achieved for a given computational budget or, conversely, by the cost reduction achieved for a given precision. Therefore a control variate quality can be assessed, with formula (4.2), from its correlation with the variable of interest and its cost: the former should be high and the latter low. Consequently, the quality of $Z_{\delta,\varepsilon}$ hinges on the choice of the

---

[10]It is actually lower triangular, with unity diagonal [see 24, th. 2.2 p. 387].

Algorithm 1: Empirical interpolation of K

Initialise $\mathcal{I}_0[K] := 0$, $R_0 := K$ and $n := 1$

while $\sup_{i \in I} \|R_n(i, \cdot)\|_{L^\infty(Y)} > \delta$ **do**

  Define $R_{n-1} := K - \mathcal{I}_{n-1}[K]$

  Compute points $i_n := \text{argmax}_{i \in I} \|R_{n-1}\|_{L^\infty(Y)}$ and $y_n := \text{argmax}_{y \in \overline{Y}} |R_{n-1}(i, y)|$

  Set $q_n := \dfrac{R_{n-1}(i_n, \cdot)}{R_{n-1}(i_n, y_n)}$

  Compute α^n by solving $\sum_{j=1}^n \alpha_j^n(i) q_j(y_p) = K(i, y_p)$, $\forall (i, p) \in I \times \{1, \dots, n\}$

  Update $\mathcal{I}_n[K] := \sum_{j=1}^n \alpha_j^n \otimes q_j$, $R_n := K - \mathcal{I}_n[K]$ and $n := n+1$

return $\tilde{K} := \mathcal{I}_n[K]$

---

couple of tolerances (δ, ε). A strategy could be devised to choose good values based on measures of cost and correlation on reasonably small samples.

Another approach to this issue would be to combine several such control variates into a variant of estimator $\theta_{n_U, n_Z}(X)$, defined by formula (4.3). Thus, for a number $n \in \mathbb{N}_*$ of control variates, we would choose $(\delta, \varepsilon) \in \mathbb{R}^n \times \mathbb{R}^n$ then observe that

$$X = \tilde{X} - \rho_1 Z_{\delta_1, \varepsilon_1} + \rho_1 \mathbb{E}(Z_{\delta_1, \varepsilon_1})$$
$$= \tilde{X} - \rho_n Z_{\epsilon_n, \delta_n} + \rho_n Z_{\epsilon_n, \delta_n} - \rho_{n-1} Z_{\epsilon_{n-1}, \delta_{n-1}} \dots + \rho_2 Z_{\epsilon_2, \delta_2} - \rho_1 Z_{\epsilon_1, \delta_1} + \rho_1 \mathbb{E}(Z_{\epsilon_1, \delta_1}). \quad (4.9)$$

Several multi-level estimators have been based on this, such as the famous multi-level Monte Carlo methods detailed in the monograph [20]. These have been applied successfully by Giles [16] and Cliffe et al. [11] to stochastic partial differential equations, with demonstrated complexity reduction. An optimal sampling strategy could then be formulated via a similar reasoning as for the two-level case, which lead to formulæ (4.5), albeit not as straightforward.

Alternatively, Peherstorfer et al. [30] proposed multi-fidelity Monte Carlo estimators, which stem from the same idea. For a sample $\omega \in \Omega^M$ of size $M \in \mathbb{N}_*$ and $n \in \mathbb{N}_*$ low-fidelity models (i.e. control variates, here), such an estimator could be

$$\frac{1}{m_0} \sum_{k=1}^{m_0} \tilde{X}(\omega_k) + \sum_{j=1}^n \left(\frac{1}{m_j} \sum_{k=1}^{m_j} Z_{\delta_j, \varepsilon_j}(\omega_k) - \frac{1}{m_{j-1}} \sum_{k=1}^{m_{j-1}} Z_{\delta_j, \varepsilon_j}(\omega_k) \right)$$

where $\forall j \in \{0, \dots, M\}$, $0 < m_j \leqslant M$. For the sake of brevity, we will note the high-fidelity model $\zeta_0 := \tilde{X}$, and $\zeta_j = Z_{\delta_j, \varepsilon_j}$ any low-fidelity model $j \in \{1, \dots, n\}$; furthermore, $\forall j \in \{0, \dots, n\}$, $\gamma_j := \text{cost}(\zeta_j)$ and $r_j = \text{corr}(\zeta_0, \zeta_j)$. Let us also introduce control coefficients $\rho \in \mathbb{R}^n$ as we did at the beginning of section 4, p. 22. We then define the multi-fidelity estimator

$$\vartheta_m(X) := \frac{1}{m_0} \sum_{k=1}^{m_0} \zeta_0(\omega_k) + \sum_{j=1}^n \rho_j \left(\frac{1}{m_j} \sum_{k=1}^{m_j} \zeta_j(\omega_k) - \frac{1}{m_{j-1}} \sum_{k=1}^{m_{j-1}} \zeta_j(\omega_k) \right). \quad (4.10)$$

Interestingly, there are results on error minimisation of such multi-fidelity estimators for a fixed budget. Owing to the telescopic sum[11] in (4.9) and (4.10), $\vartheta_m(X)$ is an unbiased estimator of $\mathbb{E}(X)$. Consequently, its mean squared error is

$$\mathbb{V}\text{ar}(\vartheta_m(X)) = \frac{\mathbb{V}\text{ar}(\zeta_0)}{m_0} + \sum_{j=1}^n \left(\frac{1}{m_{j-1}} - \frac{1}{m_j} \right) (\rho_j^2 \mathbb{V}\text{ar}(\zeta_j) - 2\rho_j \mathbb{C}\text{ov}(\zeta_0, \zeta_j)),$$

---

[11]And the fact that, $\forall j \in \{0, \dots, m\}, m_j > 0$.

which we note $E(m, \rho)$, and $\mathrm{cost}(\vartheta_m(X)) = \sum_{j=0}^n m_j \gamma_j$.

Given (δ, ε), estimator $\vartheta_m(X)$ is uniquely defined by the choice of sample sizes $m \in \mathbb{N}_*^{n+1}$ and control coefficients ρ. For a given computational budget $B \in \mathbb{R}_{+*}$, an optimal choice with respect to the estimation error would be solution to

$$\min_{m \in \mathbb{R}_{+*}^{n+1}, \, \rho \in \mathbb{R}^n} \{E(m, \rho) : \mathrm{cost}(\vartheta_m(X)) = B\}. \tag{4.11}$$

Let us make the following assumptions[12], $\forall j \in \{1, \ldots, n-1\}$:

$$m_j \geqslant m_{j+1} ;$$
$$|r_j| > |r_{j+1}| ; \tag{4.12}$$
$$\frac{\gamma_i}{\gamma_{i+1}} > \frac{r_i^2 - r_{i+1}^2}{r_{i+1}^2 - r_{i+2}^2}. \tag{4.13}$$

Under these conditions, Peherstorfer et al. [see 30, th. 3.4] proved that problem (4.11) has a unique solution $(\breve{m}, \breve{\rho})$ expressed as

$$\breve{m}_0 = B \left(\sum_{j=0}^n \sqrt{\gamma_j \gamma_0 \frac{r_j^2 - r_{j+1}^2}{1 - r_1^2}} \right)^{-1},$$

$$\forall j \in \{1, \ldots, n\}, \quad \breve{m}_j = \breve{m}_0 \sqrt{\frac{\gamma_0}{\gamma_j} \frac{r_j^2 - r_{j+1}^2}{1 - r_1^2}} \quad \text{and} \quad \breve{\rho}_j = \frac{\mathbb{C}\mathrm{ov}(\tilde{X}, Z_j)}{\mathbb{V}\mathrm{ar}(Z_j)}.$$

Then the mean squared error (i.e. variance, here) reduction achieved is[12]

$$\frac{E(\breve{m}, \breve{\rho}) p}{\mathbb{V}\mathrm{ar}(\tilde{X})} = \left(\sum_{j=0}^n \sqrt{\frac{\gamma_j}{\gamma_0} (r_j^2 - r_{j+1}^2)} \right)^2, \tag{4.14}$$

where $p := B / \mathrm{cost}(\tilde{X})$. If $p \in \mathbb{N}_*$ and $\breve{m} \in \mathbb{N}_*^{n+1}$ (see below), the left-hand side of (4.14) is $\mathbb{V}\mathrm{ar}(\theta_{\breve{m}}(X)) / \mathbb{V}\mathrm{ar}(\theta_p(\tilde{X}))$ and $\mathrm{cost}(\theta_p(\tilde{X})) = \mathrm{cost}(\theta_{\breve{m}}(X)) = B$.

In conditions (4.12) and (4.13), we see that only cost and correlation are involved; particularly, no assumption is made as to the pointwise accuracy of the approximation yielding the control variates. Moreover, the error reduction expressed in equation (4.14) shows that the contribution of one control variate depends on its correlation to the others. A strategy could be developed to choose $(\delta, \varepsilon) \in \mathbb{R}_{+*}^n \times \mathbb{R}_{+*}^n$ so as to satisfy conditions (4.12) and (4.13), in which case we would know the optimal choice $(\breve{m}, \breve{\rho})$.

It should be noted that minimisation problem (4.11) is posed over $\mathbb{R}_{+*}^{n+1} \times \mathbb{R}^n$; consequently, $\breve{m}$ will have to be projected onto $\mathbb{N}_*^{n+1}$. For a given computational budget not to be exceeded, we would use the lower integers $\lfloor \breve{m} \rfloor$, whereas we would take $\lceil \breve{m} \rceil$ in order to satisfy a given tolerance t on the mean squared error. In the latter case, Peherstorfer et al. [see 29, th. 1] has proven, under some assumptions, that $\mathrm{cost}(\vartheta_m(X)) \in \mathcal{O}(t^{-1})$; a convergence rate which, according to Cliffe et al. [11], is also achieved by multi-level Monte Carlo methods.

Finally, Peherstorfer [28] proposes an adaptive approach to account for the non-negligible creation cost of a control variate, whereas the aforementioned methods only consider the sampling cost. Its purpose is to balance the overall budget between construction and evaluation of a single

---

[12]With the convention $r_{n+1} := 0$.

surrogate model, so that the model design is cost-oriented as well. This too could be adapted to the method proposed here, although there is not so much a "construction-evaluation"[13] cost separation as an "initialisation-asymptotic" one; the former refers to the library construction cost and the latter to the evaluation cost once the library has reached practical completion.

4.3   Numerical results

We consider bidimensional problems of type (2.1) and choose three different random stationary conductivities K. The first one is an ideal quasi-periodic case previously introduced in subsection 3.2, with a conductivity of rank at most 2; it falls within the scope of the control variate technique detailed in subsection 4.1.2 and allows us to compare it to the one from subsection 4.2. Both other conductivities where chosen to assess the limits of this latter technique and have almost surely full rank[14]. The first one still follows a regular mesoscopic grid whereas the last one exhibits no such structure.

For each test case we wish to estimate the total cost reduction from computing $\theta^\eta(K_\star^N)$ to computing $\theta^\eta(X)$ for different controlled versions X of $K_\star^N$ and always for the same standard deviation $\eta := 0.1$. Those total costs are respectively $C_{FE} = \hat{c}_n \mathbb{V}\mathrm{ar}(K_\star^N)/\eta^2$, and $C_X = (\hat{c}_n + c_Z)n_U + c_Z n_Z$ where $\hat{c}_n$ and c_Z are the costs of a single estimation of $K_\star^N$ and of the control variate[15] Z involved in X, respectively; n_U and n_Z are calculated according to formulæ (4.5). Single costs, variances and covariances are estimated from 100 samples of $K_\star^N$, X and Z. $X_{\delta,\varepsilon}$ is tested with five values of (δ, ε) on each test case, and X_1 and X_2 are tested on the first test case.

All tests are set on a domain $D := [0, 20]^2 \equiv \{1, \ldots, 400\} \times [0, 1]^2$. Control variates are evaluated by MsLRM with $\dim(V_h(Y)) := 441$ and EIM cost is accounted for, albeit lower than $0.1\,\mathrm{s}$ per interpolation. $K_\star^N$ is computed by FEM with the same mesh as MsLRM, thus $160\,801$ degrees of freedom[16]; its associated cost $\hat{c}_n \approx 246\,\mathrm{s}$ does not vary significantly from one test case to another.

These computations were run on the same hardware as described at the beginning of subsection 3.2, p. 11.

4.3.1   Quasi-periodic inclusions

The first case is defined in equation (3.4) and illustrated on figure 4a; we set defect probability $p := 0.5$ for greatest periodicity loss. Table 6 displays the cost reductions achieved with various control variates, along with values on which this cost reduction depends. This table has been designed so that greater values mean better performance, except for the average ranks r_w and $r_{\bar{K}}$, respectively for correctors and empirically interpolated conductivities. The single cost reduction $\hat{c}_n/c_Z$ was irrelevant for Z_1 and Z_2 whose evaluation cost is almost zero, so we display instead $\hat{c}_n/c_p$ between parentheses, where c_p is the a priori cost discussed in subsection 4.1.2 (either c_{p1} or c_{p2}, respectively); those computations were performed by MsLRM with tolerance $\varepsilon := 0.01$. The other values between parentheses are the optimal variance reductions, estimated from formula (4.2); the difference between those and the observed reductions comes from the uncertainties in empirical estimations of variances and covariances.

The first observation is that all control variates achieve comparable variance reduction, and therefore the major difference is in their cost. Hence Z_1 and Z_2 are the most efficient by far and the cost reduction displayed is only limited by the fact that we always do at least one computation of $K_\star^N$ (i.e. $n_U \geqslant 1$). Here the variance reduction is such that every control variate achieved

---

[13]Sometimes referred to as "offline-online".
[14]I.e. $r_K = N^2$.
[15]Either Z_1, Z_2 or some $Z_{\delta,\varepsilon}$, depending on the chosen surrogate model.
[16]Slightly less than $400 \times 441 = 176\,400$, due to continuity.

Table 6: Cost and variance reductions on quasi-periodic inclusions — $\mathbb{V}\mathrm{ar}(K_\star^N) = 1.8$

δ	ε	$r_{\tilde{K}}$	r_w	$\hat{c}_n/c_Z$	$\mathbb{V}\mathrm{ar}(K_\star^N)/\mathbb{V}\mathrm{ar}(X)$		n_Z/n_U	C_{FE}/C_X
$-Z_1-$	0.01	–	1	(59)	10 747	(10 747)	3337	180
$-Z_2-$	0.01	–	11	(0.11)	15 673		461	178
1	1	1	1	165	10 751	(11 335)	209	79.3
1	0.1	1	1	164	10 751	(11 335)	209	79.1
1	0.01	1	7.2	134	2054	(2392)	208	70.5
0.1	1	2	1	140	15 327	(15 503)	208	72.3
0.01	1	2	1	140	15 327	(15 503)	208	72.3

Table 7: Cost and variance reductions on regular peaks — $\mathbb{V}\mathrm{ar}(K_\star^N) = 1.2$

δ	ε	$r_{\tilde{K}}$	r_w	$\hat{c}_n/c_Z$	$\mathbb{V}\mathrm{ar}(K_\star^N)/\mathbb{V}\mathrm{ar}(X)$		n_Z/n_U	C_{FE}/C_X
1	1	22.7	1	29	15	(17)	16	5.9
1	0.1	22.7	23.9	8.29	1307	(1367)	66	6.6
0.1	1	35.3	1	19	15	(18)	13	5.0
0.01	1	49.5	1	14	15	(18)	11	4.3

$n_U = 1$, and Z_1 and Z_2 reduced the total cost to that single computation: $C_X \approx \hat{c}_n$. This ignores the a priori cost which, although low for Z_1, is much greater for Z_2 and makes it questionable whether the additional variance reduction is worth the extra cost[17]. These a priori costs were significantly reduced by using MsLRM instead of FEM: the values of $\hat{c}_n/59$ and $9\hat{c}_n$ would have been, respectfully, $2\hat{c}_n$ and $2(N^2 + 1)\hat{c}_n = 802\hat{c}_n$ with FEM.

As for $Z_{\delta,\varepsilon}$, ε has little effect (except a cost increase) but δ makes the difference between a rank-1 approximation $\tilde{K}$, which yields the same variance reduction as the first-order control variate Z_1, and the exact rank-2 conductivity from which we get the same variance reduction as with the second-order control variate Z_2. There is hardly any difference in cost between the cases where $r_{\tilde{K}} = 1$ and those where $r_{\tilde{K}} = 2$, c_Z varies only from 1.5 s to 2 s. Because every $Z_{\delta,\varepsilon}$ reaches the optimal situation $n_U = 1$ here, the differences in total cost reduction C_{FE}/C_X is not significant and one should rather gauge performance from the variance reduction $\mathbb{V}\mathrm{ar}(K_\star^N)/\mathbb{V}\mathrm{ar}(X)$.

4.3.2 Regular peaks

The second conductivity tested exhibits a mesoscopic structure following a regular grid, yet it is aperiodic in the sense that its rank almost surely equals the number of cells. Its expression is

$$K(i, y, \omega) = 1 + \alpha_i(\omega)e^{-\|\beta_i(\omega)(y-\gamma)\|}$$

where $\alpha_i \in \mathcal{U}([0, 199])$ and $\beta_i = \mathrm{diag}((\beta_{i,1}, \beta_{i,2}))$ with $(\beta_{i,1}, \beta_{i,2}) \in \mathcal{U}([2, 10])^2$. The exponential peak is centred within each cell with $\gamma := (0.5, 0.5)$. An example of this function is displayed on figure 16a. Its contrast (between highest and lowest values) and variance are on a par with the previous conductivity, yet its periodicity is much lower.

Results are presented in table 7 in the same format as table 6 previously explained, yet without Z_1 and Z_2 which cannot be used here. We first observe that a cost reduction is achieved for

---

[17]Ignoring the influence of the complementary reference periodic material would half this extra cost but reduce correlation.

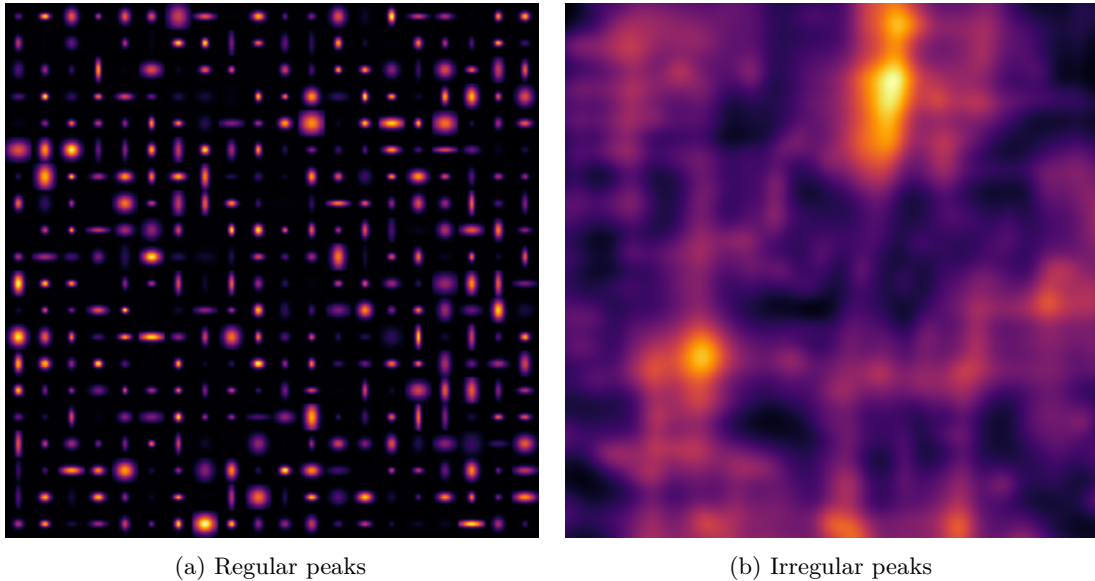(a) Regular peaks   (b) Irregular peaks

Figure 16: Examples of second and third test conductivity functions on a 20×20 grid

every value of (δ, ε) tested but $(1, 0.01)$. The results for this latter case are not available since the approximation reached ranks so high ($r_w \geqslant 100$) that the test machine ran out of memory[18]; these computations were costlier than the FEM ones and serve to point out MsLRM limits. Then we see that a low tolerance δ yields better results since a high conductivity is quite detrimental to MsLRM performance and does produce a better correlated control variate. Indeed, 23 is already a great rank increase from the previous test case, although much better than the raw $r_K = 400$. Finally, performance improves when ε is lowered just enough[19] to go beyond the crude rank-1 approximation of the correctors.

4.3.3   Irregular peaks

This last conductivity function has been chosen to be an irregular variant of the second one, with similar exponential peaks distributed according to a stationary Poisson point process. It reads

$$K(x, \omega) = 1 + \sum_{n=1}^{\nu(\omega)} \alpha_n(\omega) e^{-\|\beta_n(\omega)(x - \gamma_n(\omega))\|}$$

where the families (α_n) and (β_n) are composed of independent and identically distributed random variables: $\alpha_n \in \mathcal{U}([0, 179])$ and $\beta_n = \mathrm{diag}((\beta_{n,1}, \beta_{n,2}))$ with $(\beta_{n,1}, \beta_{n,2}) \in \mathcal{U}([0.1, 2])^2$. The number of peaks ν follows a Poisson distribution of expectation $(N + R)^2$. R is defined as the

---

[18]Memory usage went over $8\,\mathrm{GiB}$.
[19]Here, a better compromise could be found with $\varepsilon \in\,]0.1, 1[$.

Table 8: Cost and variance reductions on irregular peaks — $\mathbb{V}\mathrm{ar}(K_\star^N) = 3642$

δ	ε	$r_{\bar{K}}$	r_w	$\hat{c}_n/c_Z$	$\mathbb{V}\mathrm{ar}(K_\star^N)/\mathbb{V}\mathrm{ar}(X)$		n_Z/n_U	C_{FE}/C_X
1	1	28.7	19.8	11.1	4628	(8226)	237	10.0
1	0.1	28.7	45.4	3.15	4624	(8276)	139	3.0
1	0.01	28.7	72.9	1.13	4623	(8275)	100	1.1
0.1	1	41.8	19.6	9.42	4822	(8796)	225	8.6

radius beyond which a peak's value is below tolerance δ, hence

$$\left\| \alpha_n e^{-\left\| \beta_n \times {}^t(R,R) \right\|} \right\|_{L^\infty(\Omega)} \leqslant \delta,$$

$$\text{so } R := \lambda_{min}(\beta_n)^{-1} \ln\left(\frac{\|\alpha_n\|_{L^\infty(\Omega)}}{\delta} \right) = 10 \ln\left(\frac{179}{\delta} \right)$$

$$\text{with } \lambda_{min} = \min_{\omega \in \Omega} \min\{\beta_{n,1}(\omega), \beta_{n,2}(\omega)\}.$$

The centres γ_n are independent random variables following the same uniform law $\mathcal{U}([-R, N+R]^2)$. This represents the truncation to $D := [0,N]^2$ of a spatial Poisson point process over $\mathbb{R}^2$, accounting for a radius R around each point. An example of such K is illustrated on figure 16b.

The results in table 8 follow the same layout as the previous one. Surprisingly, the results are somewhat better than those reported in subsection 4.3.2, even though the average of $r_{\bar{K}}$ is slightly higher. As before, every control variate tested reduces the overall cost but $Z_{1,0.01}$, which does not offer further variance reduction than $Z_{1,0.1}$. Unlike the previous case, $Z_{1,1}$ goes beyond the rank-1 approximations of the correctors and is the best control variate here since it achieves almost as good a variance reduction as $Z_{1,0.1}$. We conclude that a crude empirical interpolation of the conductivity along with low-rank (but above the trivial rank 1) approximation of the correctors yields significant cost-reduction (factor 10 for $Z_{1,1}$).

Another important parameter to discuss here would be the mesoscopic discretisation. Although the choice was obvious for every other test case presented, it was arbitrary for this one. A different cell size based, for example, on the radius R might be more relevant.

5   Conclusion

We proposed a way to reduce the cost of stochastic homogenisation for quasi-periodic conductivities by a low-rank approximation of the corrector functions identified with bivariate functions. The subsequent error on the homogenised quantities has been found to be reasonable on our examples, whereas the computational cost is greatly reduced in most cases, compared to FEM. The complexity was reduced first regarding domain size and then to samples number. The major influence on the cost of this multiscale low-rank method [MsLRM, from 5] comes from the rank of the conductivity identified as a tensor; the closer to a periodic function, the lower the rank.

Interestingly, the number of occurrences of a given defect does not change the conductivity rank and therefore has no effect on the complexity of the associated corrector problem. More generally, materials that would not be intuitively considered quasi-periodic have been found to be of low complexity for this MsLRM. A category of such materials is quasi-periodic ones transformed through a random mapping with low rank gradient. Another one is materials following a regular grid and whose grid cells patterns are linear combinations of the same small number of patterns.

This reduced complexity for aperiodic media with mesoscopic structure was exploited by building a low-rank empirical interpolation of the conductivity, computing MsLRM approximations of the associated corrector functions and using the resulting homogenised operator as a control variate to the homogenised operator computed by direct FEM. This was found to provide cost-efficient and well correlated control variates in our numerical experiment, not only for quasi-periodic conductivities but also for materials with not enough periodicity for the MsLRM to be efficient. We illustrated and discussed the influences of tolerances on both empirical interpolation on the conductivity and low-rank approximation of the correctors. Additionally, the MsLRM reduced greatly the a priori cost of the weakly stochastic control variate from Legoll and Minvielle [22], which is more specific but less expensive.

Finally, this variance reduction technique, applied here to quantities computed by FEM, could be used in an experimental campaign on measured quantities, with sufficient knowledge of the material to deduce a low-rank approximation of the conductivity as described in subsection 4.2.

Acknowledgement

References

[1] Assyr Abdulle, Weinan E, Björn Engquist, and Eric Vanden-Eijnden. "The heterogeneous multiscale method". In: *Acta Numerica* 21 (2012). DOI: 10.1017/S0962492912000025.

[2] Arnaud Anantharaman and Claude Le Bris. "Elements of mathematical foundations for a numerical approach for weakly random homogenization problems". 2010.

[3] Arnaud Anantharaman and Claude Le Bris. "Homogénéisation d'un matériau périodique faiblement perturbé aléatoirement". In: *Comptes Rendus Mathematique* 348.9-10 (May 2010), pp. 529–534. ISSN: 1631073X. DOI: 10.1016/j.crma.2010.03.001.

[4] Arnaud Anantharaman and Claude Le Bris. "A numerical approach related to defect-type theories for some weakly random problems in homogenization". In: *Multiscale Modeling & Simulation* (2011). arXiv: arXiv:1005.3910v1.

[5] Quentin Ayoul-Guilmard, Anthony Nouy, and Christophe Binetruy. "Tensor-based multiscale method for diffusion problems in quasi-periodic heterogeneous media". In: *ESAIM Mathematical Modelling and Numerical Analysis* to appear (2018). DOI: 10.1051/m2an/2018022.

[6] Maxime Barrault, Yvon Maday, Ngoc Cuong Nguyen, and Anthony T. Patera. "An 'empirical interpolation' method: application to efficient reduced-basis discretization of partial differential equations". In: *Comptes Rendus Mathematique* 339.9 (2004), pp. 667–672. ISSN: 1631-073X. DOI: 10.1016/j.crma.2004.08.006.

[7] G. D. Birkhoff. "Proof of the Ergodic Theorem". In: *Proceedings of the National Academy of Science* 17 (1931), pp. 656–660. DOI: 10.1073/pnas.17.12.656.

[8] Xavier Blanc, Claude Le Bris, and Pierre-Louis Lions. "Une variante de la théorie de l'homogénéisation stochastique des opérateurs elliptiques". In: *Comptes Rendus Mathematique* 343.11-12 (Dec. 2006), pp. 717–724. ISSN: 1631073X. DOI: 10.1016/j.crma.2006.09.034.

[9] Xavier Blanc, Claude Le Bris, and Pierre-Louis Lions. "Stochastic homogenization and random lattices". Apr. 2007.

REFERENCES

[10]   Alain Bourgeat and Andrey Piatnitski. "Approximations of effective coefficients in stochastic homogenization". In: *Annales de l'Institut Henri Poincare (B) Probability and Statistics* 40.2 (Apr. 2004), pp. 153–165. ISSN: 02460203. DOI: `10.1016/j.anihpb.2003.07.003`.

[11]   K A Cliffe, M B Giles, R Scheichl, and A L Teckentrup. "Multilevel Monte Carlo methods and applications to elliptic PDEs with random coefficients". In: *Computing and Visualization in Science* 14.1 (Aug. 2011), p. 3. ISSN: 1433-0369. DOI: `10.1007/s00791-011-0160-x`.

[12]   Ronan Costaouec, Claude Le Bris, and Frédéric Legoll. "Approximation numérique d'une classe de problèmes en homogénéisation stochastique". In: *Comptes Rendus Mathematique* 348.1-2 (2010). DOI: `10.1016/j.crma.2009.10.027`.

[13]   Anneliese Defranceschi. "An introduction to homogenization and G-convergence". In: *School on Homogenization.* 1993, pp. 1–48.

[14]   Daniele Antonio Di Pietro and Alexandre Ern. *Mathematical Aspects of Discontinuous Galerkin Methods.* Vol. 69. Springer Science & Business Media, 2011. ISBN: 3642229808.

[15]   Yalchin Efendiev and Thomas Y. Hou. *Multiscale Finite Element Methods.* Surveys and Tutorials in the Applied Mathematical Sciences. New York, NY: Springer New York, 2009. ISBN: 978-0-387-09495-3. DOI: `10.1007/978-0-387-09496-0`.

[16]   Michael B Giles. "Multilevel Monte Carlo Path Simulation". In: *Operations Research* 56.3 (2008), pp. 607–617. DOI: `10.1287/opre.1070.0496`.

[17]   Antoine Gloria and Felix Otto. "An optimal variance estimate in stochastic homogenization of discrete elliptic equations". In: *The Annals of Probability* 39.3 (May 2011), pp. 779–856. ISSN: 0091-1798. DOI: `10.1214/10-AOP571`. arXiv: `arXiv:1104.1291v1`.

[18]   Antoine Gloria and Felix Otto. "An optimal error estimate in stochastic homogenization of discrete elliptic equations". In: *The Annals of Applied Probability* 22.1 (Feb. 2012), pp. 1–28. ISSN: 1050-5164. DOI: `10.1214/10-AAP745`. arXiv: `arXiv:1203.0908v1`.

[19]   Antoine Gloria, Felix Otto, and Stefan Neukamm. "Quantification of ergodicity in stochastic homogenization : optimal bounds via spectral gap on Glauber dynamics". In: *Inventiones mathematicae* 199.2 (2015), pp. 455–515. ISSN: 0020-9910. DOI: `10.1007/s00222-014-0518-z`.

[20]   Stefan Heinrich. "Multilevel Monte Carlo Methods". In: *Large-Scale Scientific Computing.* Ed. by Svetozar Margenov, Jerzy Waśniewski, and Plamen Yalamov. Berlin, Heidelberg: Springer Berlin Heidelberg, 2001, pp. 58–67. ISBN: 978-3-540-45346-8.

[21]   V. V. Jikov, S. M. Kozlov, and O. A. Oleinik. *Homogenization of Differential Operators and Integral Functionals.* Vol. 10.1007/97. Springer-Verlag, 1994. ISBN: 978-3-642-84661-8. DOI: `10.1007/978-3-642-84659-5`.

[22]   Frédéric Legoll and William Minvielle. "A Control Variate Approach Based on a Defect-Type Theory for Variance Reduction in Stochastic Homogenization". In: *Multiscale Modeling and Simulation* 13.2 (2015). DOI: `10.1137/140980120`.

[23]   Frédéric Legoll and Florian Thomines. "On a variant of random homogenization theory: convergence of the residual process and approximation of the homogenized coefficients". In: *ESAIM Mathematical Modelling and Numerical Analysis* 48.2 (2014). DOI: `10.1051/m2an/2013111`.

[24]   Yvon Maday, Ngoc Cuong Nguyen, Anthony T. Patera, and George S. H. Pau. "A general multipurpose interpolation procedure: the magic points". In: *Communications on Pure & Applied Analysis* 8.1 (2009), pp. 383–404. DOI: `10.3934/cpaa.2009.8.383`.

REFERENCES

[25] François Murat. "Compacité par compensation". In: *Annali della Scuola Normale Superiore di Pisa - Classe di Scienze* 5.3 (1978), pp. 489–507.

[26] François Murat, Luc Tartar, Doina Cioranescu, L. Gibiansky, A. Cherkaev, and K. Lurie. *Topics in the mathematical modelling of composite materials.* Ed. by A Cherkaev and Robert Kohn. Springer, 1997. ISBN: 9781461273905.

[27] Gabriel Nguetseng. "A General Convergence Result for a Functional Related to the Theory of Homogenization". In: *SIAM J. Math. Anal.* 20.3 (May 1989), pp. 608–623. ISSN: 0036-1410. DOI: 10.1137/0520043.

[28] Benjamin Peherstorfer. *Multifidelity Monte Carlo estimation with adaptive low-fidelity models.* Tech. rep. University of Wisconsin-Madison, 2017.

[29] Benjamin Peherstorfer, Max Gunzburger, and Karen Willcox. "Convergence analysis of multifidelity Monte Carlo estimation". In: *Numerische Mathematik* (2018).

[30] Benjamin Peherstorfer, Karen Willcox, and Max Gunzburger. "Optimal Model Management for Multifidelity Monte Carlo Estimation". In: *SIAM Journal on Scientific Computing* 38.5 (2016). DOI: 10.1137/15M1046472.

[31] Benjamin Peherstorfer, Karen Willcox, and Max Gunzburger. "Survey of multifidelity methods in uncertainty propagation, inference, and optimization". In: *SIAM Review* to appear (2018).

[32] Sergio Spagnolo. "Sulla convergenza di soluzioni di equazioni paraboliche ed ellittiche". In: *Ann. Scuola Norm. Pisa. Cl. Sci.* 4.22 (1968), pp. 571–597.

[33] Luc Tartar. "Compensated compactness and applications to partial differential equations". In: *Nonlinear analysis and mechanics, Heriot-Watt symposium* 4 (1979), pp. 136–211.

[34] Florian Thomines. "Méthodes mathématiques et techniques numériques de changement d'échelle : application aux matériaux aléatoires". PhD thesis. École des Ponts ParisTech, 2012.